

# **FULL and ROW THGEM characterization**

G.A. Brischetto, I. Ciraldo, D. Torresi

26 March 2020

## **Abstract**

In the present report the characterization of the tracker prototype using different kind of THGEM is described. The main parameters that have been explored are: the THGEM voltage, the drift voltage, the induction voltage, the gas pressure and the rate of the incident particles.

# Chapter 1

## Experimental setup

The gas tracker have been tested in a gas chamber located along the TeBe beam line that is shown in Fig. 1.1. The gas chamber is isolated from the high vacuum beam line by mean of a thin Mylar window ( $2.5$  or  $6\ \mu m$  thick) or by a few mm thick aluminum plate. This last is used just during the test with  $\alpha$ -source that is located inside the gas chamber itself. The gas chamber is located at an angle of  $30^\circ$  respect to the beam direction. The window is located at about  $47$  cm from the target position. The window is **120 mm large and 100 mm high.**

A slow control system allow to fill the gas chamber with at a given pressure with a constant flux of gas up to  $145$  sccm<sup>1</sup>. Up to now all the test have been performed using isobutane ( $C_4H_{10}$ ) with a purity of  $99.95\%$  at four different pressure:  $10$ ,  $20$ ,  $30$  and  $40$  mbar and with the maximum available flux, i.e.  $145$  sccm.

The alpha source used during the test is the a  $55\ kBq$   $^{241}Am$  source. A shutter remotely controlled is used to allow (open) or prevent (close)  $\alpha$ -particles from enter the tracker.

The rate of  $\alpha$ -particles entering the tracker after the shutter is  $140$  pps (particles per second), the shutter cut a solid angle of  $3.2 \cdot 10^{-2}$  sr corresponding to a cone with an opening angle<sup>2</sup> of  $\theta/2 = 7.26^\circ$ .

To supply the required voltages a CAEN system on a CAEN SY5527 mainframe with an A1515 board is used (see Sec. 1.2.1). This system allows also the measurements of the currents flowing in each the power unit.

Due to the low sensitivity of the ammeter integrated in the CAEN power supply a more sensitive picoammeter have been used, it is called PICO and

---

<sup>1</sup>Standard Cubic Centimeter per Minute.

<sup>2</sup>It is the angle between the axis and the border.

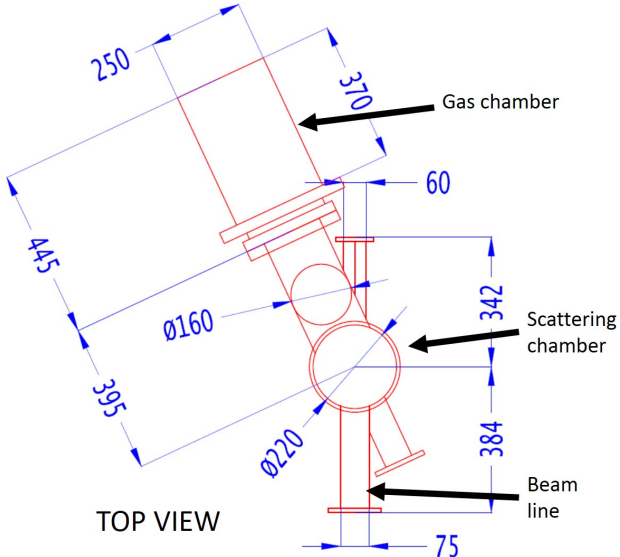


Figure 1.1: Sketch of the TeBe beam line.

it was designed and built at INFN-NA. It is capable to measure the currents with an accuracy of the order of tenth of pA while the integrated CAEN ammeter has an accuracy of about 2 nA.

## 1.1 Tracker prototype

The tracker prototype consists in one module (one of the 8 final modules) that has the same structure as the final FPD but is smaller in the dispersive direction.

The active volume of the detector is  $107 \times 107 \times 185$  mm<sup>3</sup>. While the full size nothing excluded is of about  $180 \times 200 \times 215$  mm<sup>3</sup>.

An electric scheme of the prototype is shown in Figure 1.2.

The **drift region**, delimited by the cathode and the multiplication stage, is 185 mm deep, it is designed to set a uniform electric field. A partition made of 35 double rings of wires connect the edge of the cathode with the edge of the multiplication region. The rings are 5 mm distant and in between there are four 10 MΩ resistors connected in parallel so the resistance is 2.5 MΩ. The total resistance of the partition is 87.5 MΩ. The presence of this partition generate a current of several  $\mu$ A in the cathode and in the bottom of the THGEM also in steady condition (i.e. no particles crossing the drift region). The drift region is filled with gas at low pressure (10-100 mbar). The gas filling the drift region should have a high drift velocity in order to guarantee a fast collection of the charge and should manifest a saturation of the drift velocity with the electrical field applied.

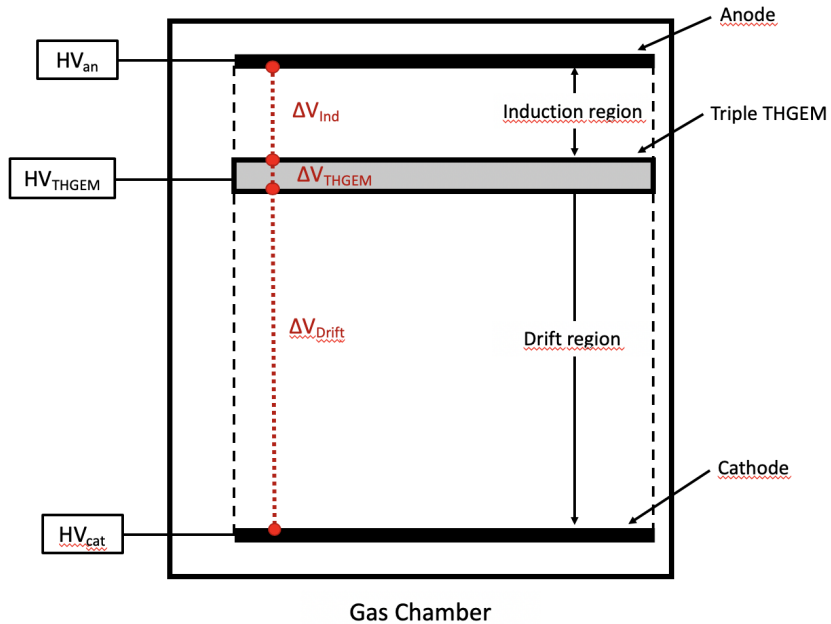


Figure 1.2: Sketch of the Prototype.

The **multiplication stage** is based on multiple THGEM, described in the next subsection.

The **induction region** is delimited by the top of the THGEM and the anode and is 1 mm deep. The electrons emerging from the multiplication region are directed towards a segmented anode made of 144 strips  $750 \mu\text{m}$  large<sup>3</sup>. Anyway during the test with ammeter the segmented anode was replaced by an not-segmented anode, that is a whole metallized layer with the same mechanical size of the segmented anode.

## 1.2 THGEM

Two multiple THGEM have been used in the test. Both of them are made of three layers, but they show different hole pattern and also different executive details since have been produced by two different manufacturers. In the first one, referred to as FULL THGEM **F10** (Figure 1.4(a)), the holes are uniformly distributed over the active surface; in the second one, called ROW THGEM **R1** (Figure 1.5(a)), the holes are arranged in five rows. The main characteristics of the two prototypes are shown in Table 1.1. The main difference are: the hole pattern, the thickness of the board, the size of the rim and the diameter of the hole.

---

<sup>3</sup>The capacitance of a single strip is roughly 22 pF.

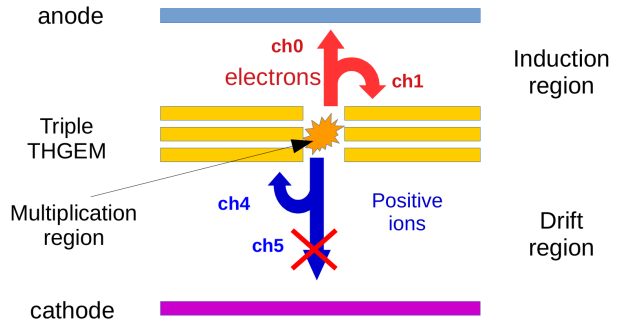


Figure 1.3: Cartoon of the flows of positive ions and electrons in the tracker prototype.

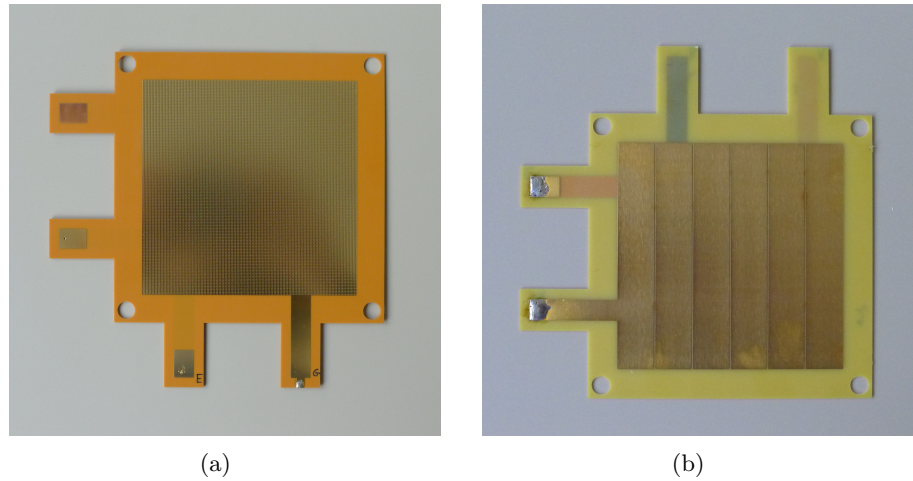


Figure 1.4: Pictures of the FULL THGEM (a) and the ROW THGEM (b).

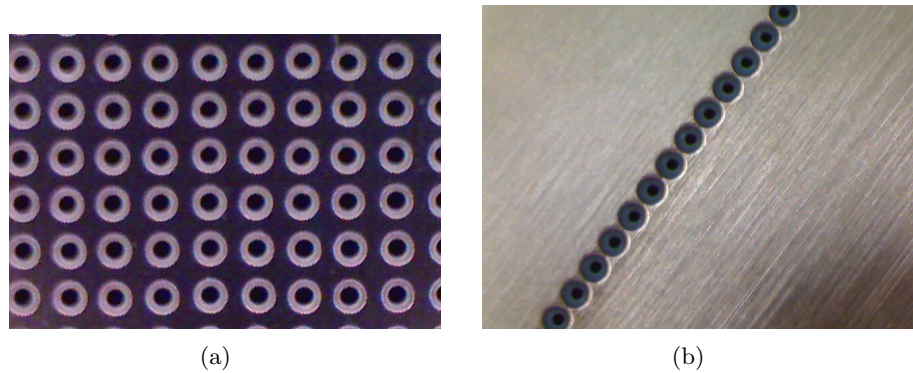


Figure 1.5: A magnification of the THGEM that show the different hole patterns: (a) FULL THGEM, (b) ROW THGEM.

	<b>F10</b>	<b>R1</b>
Substrate material*	Ceramic SD103K	PCB
Finish board thickness* [mm]	$1.4 \pm 0.1$	1.28
Dimension [mm <sup>2</sup> ]	$107 \times 107$	$107 \times 107$
Rim size* [mm]	0.1	0.2
Rows	$143 \times 143$	5
Holes	20449	143
Hole diameter* [mm]	$0.30 \pm 0.05$	0.280
Hole spacing	0.75	0.75

Table 1.1: The main characteristics of the two type of THGEM tested. The star highlights the characteristics that are different between the two THGEM.

### 1.2.1 The CAEN bias Supply and PICO

The power supply of the prototype is based on a *Universal Multichannel Power Supply System SY5527LC*<sup>4</sup> and an *Individual Floating Channel Dual Range Boards for Quadruple and Triple GEM detectors A1515*<sup>5</sup>. A scheme of the bias is shown in Fig. 1.6(a). In Fig. 1.2 a very simple scheme of the flows of positive ions and electrons is shown. The two ammeters: the CAEN ammeter integrated in the power supply (in the following just CAEN ammeter) and PICO do not measure exactly the same currents as illustrated in Fig. 1.8. In fact the CAEN ammeter measures the currents that flows in the branch where is the power supply while the PICO ammeter measures the current flowing in the branch where are the electrodes. The six measured currents are: anode, top3, bot3/top2, bot2/top1, bot1 and cathode as shown in Figure 1.7. For the sake of clarity we underline that top 3 corresponds to the top layer of the 3-layers stack of THGEM, i.e. that one looking to the anode while bot 1 is the bottom layer of the stack, i.e. that one looking to the cathode. Bot3/top2 as well bot2/top1 refers to the metallic layers embedded in the THGEM stack. In no case currents in these two electrodes have been observed.

The current read with PICO for bot 1 has usually a worse accuracy. This is due to the fact that PICO has two dynamical ranges with two related accuracy. Since in bot1 flow a large current due to the partition wires (see 1.1) the dynamical range of PICO is the largest for such electrode and

---

<sup>4</sup><https://www.caen.it/products/sy5527lc/>

<sup>5</sup><https://www.caen.it/products/a1515/>

therefore the accuracy is worse<sup>6</sup>.

### 1.3 Method

The main parameters that determine the behaviour of the detector are: gas pressure, voltage of the THGEM ( $V_{THGEM}$ ), voltage of the induction region ( $V_{ind}$ ) and voltage of the drift region ( $V_{drift}$ ). The cathode cannot be kept connected at ground if we want to measure the current flowing on it, therefore the anode was kept at voltage fixed to an arbitrary value of 20 V (see Fig. ??). This value should not affect the measurements of the currents of any electrodes.

The method consists in keeping fix all the parameter but one and to measure all the currents of all the electrodes varying just the parameters left free to change. For example we keep fix the gas pressure the  $V_{drift}$ ,  $V_{ind}$ , while the  $V_{THGEM}$  was changed a small step. In this way we get 6 plots as a function of  $V_{THGEM}$ , one for each current i.e. anode, bot1, bot2/top1, bot3/top2, top3 and cathode. A run lasts usually 180 s (see Fig. 1.8):

- 60 s with shutter closed;
- 90 s with shutter open;
- 30 s with shutter closed.

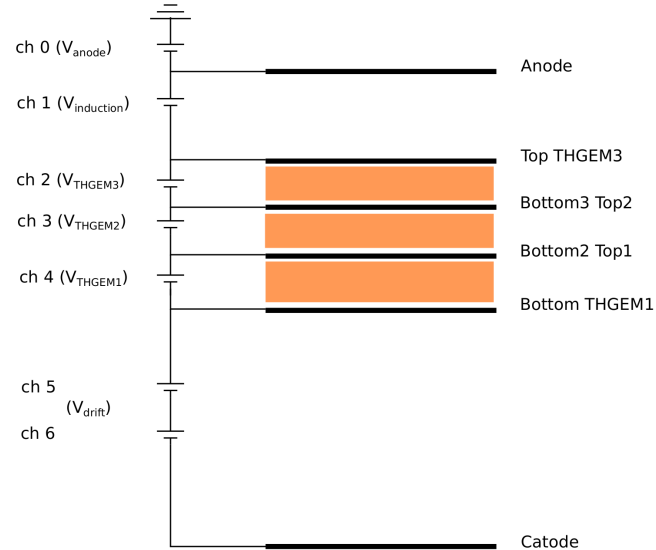
An average of the current flowing during the first 60 s (shutter closed) and an average during the 90 s with shutter open is performed. The difference between the two measurements with shutter open and closed gives the actual current associated to the  $\alpha$ -particles entering the detector. In this way any dark current coming from the detector or from the ammeter is subtracted<sup>7</sup>.

In Figure 1.8 a comparison of the same run measured using the two ammeters is shown. It is evident the better accuracy of PICO.

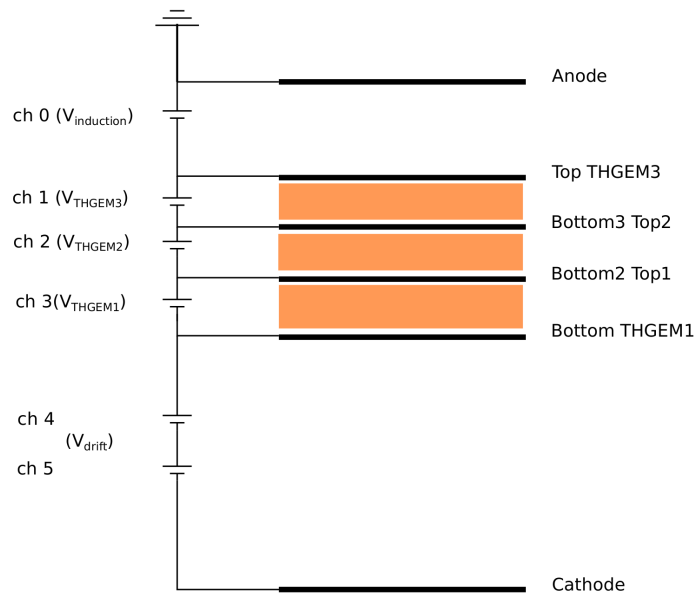
---

<sup>6</sup> Also in cathode flows a current equal to bot1 but with an opposite charge but the two dynamical ranges are different for positive and negative currents. Therefore the current flowing in the bot1 is enough to switch the dynamical range for the bot1 channel but not enough to switch the dynamical range for the cathode channel. This is why the bot 1 and cathode measure the same current in absolute value but have different accuracies.

<sup>7</sup> A possible source of dark current is due to the X-ray produced by the  $\alpha$ -source that are not stopped by the shutter.



(a)



(b)

Figure 1.6: Scheme of the Bias supply during the measurements with electronics a) and for the current measurements b).

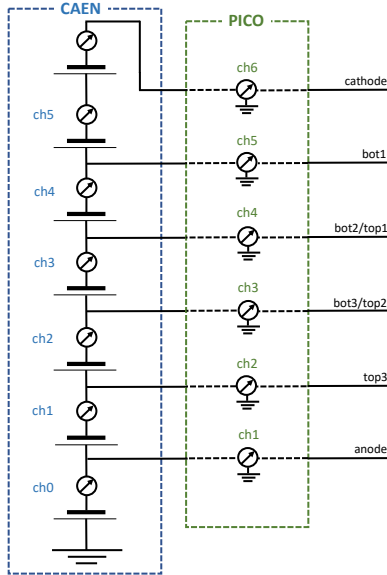


Figure 1.7: Current reading scheme for the two ammeters.

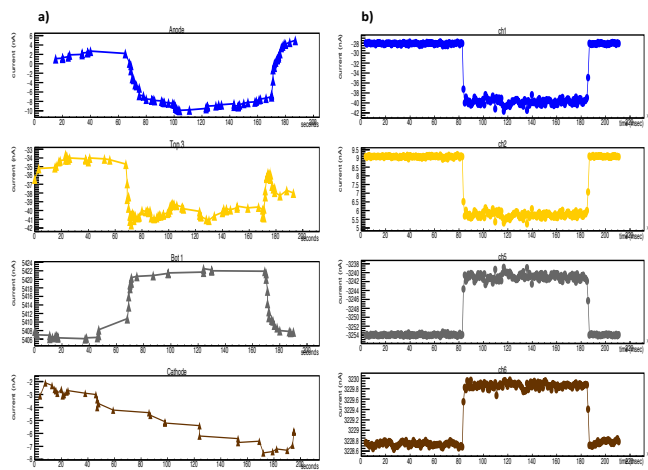


Figure 1.8: Anode, Top3, Bot1 and Cathode currents measured with CAEN ammeter a) and PICO b).

# Chapter 2

## Measurements

This section contain a description of the current measurements that was performed. It is organized as follow. First are presented the measurements with the Full THGEM and after those with the Row THGEM. For each THGEM are presented in the following order the scan of the induction The scan of the THGEM and eventually the scan of the Drift.

A separate section is devoted to the study of the in-beam test.

### 2.1 test with $\alpha$ -source

#### 2.1.1 FULL THGEM

The FULL THGEM was made by the xxx manufacturer. Their characteristics are summarized in Tab. 1.1.

##### Scan on $\Delta V_{ind}$

In this subsection a series of systematic measurements were performed to study the effects of the variation of the voltage  $\Delta V_{ind}$  on all the measured currents. These measurements were done at different pressures (P) and values of  $\Delta V_{TH}$  and  $\Delta V_{drift}$ , a summary scheme of the configurations is shown in Table 2.1. The  $\Delta V_{ind}$  scans were carried out starting from 0 V and increasing the voltage by 10 or 20 V per run, until the discharge value is reached. This value is dependent on the gas pressure and possibly on the values set for  $\Delta V_{TH}$  and  $\Delta V_{drift}$ . The values at which discharge occurs are 220, 200 and 150 V for 30, 20 and 11 mbar respectively.

A typical example of the scan is shown in Figure 2.1, it corresponds at 30 mbar and  $\Delta V_{TH} = 220$  V. By raising the value of  $\Delta V_{ind}$ , the anodic current (blue line) increases, while the top3 current (yellow line) decreases approaching zero. The orange points corresponds to the sum of the currents read in top3 and anode, that is to the total negative charge (TNC)

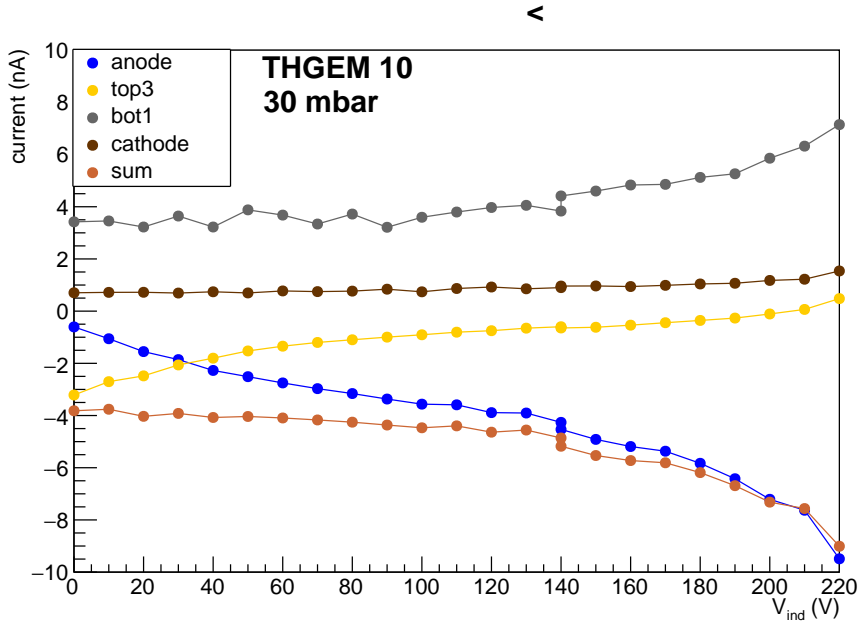


Figure 2.1: Currents measured during the scan on the voltage  $\Delta V_{ind}$  across the induction region at 30 mbar and with  $\Delta V_{TH} = 220$  V.

produced by the THGEM. Up to 140 V, The TNC is approximately constant, for values higher than 140 V the TNC increases. This simply means that the stronger is the electric field in the induction region, the greater is the fraction of secondary electrons collected at the anode and lower is the fraction of the electrons collected by the top3 electrode. For  $\Delta V_{ind}$  greater than 140 V, the TNC increases: this behaviour can be explained assuming that, when the voltage is high enough, the multiplication region extends out of the THGEM holes, expanding in the induction region (see Fig. 2.2 for

P (mbar)	$\Delta V_{TH}$ (V)	$\Delta V_{drift}$ (V)	
30.2	220	1000	5-28
30.4	200	1000	61-75
30.4	230	1000	76-89
20.5	200	1000	90-111
11	170	600	146-168

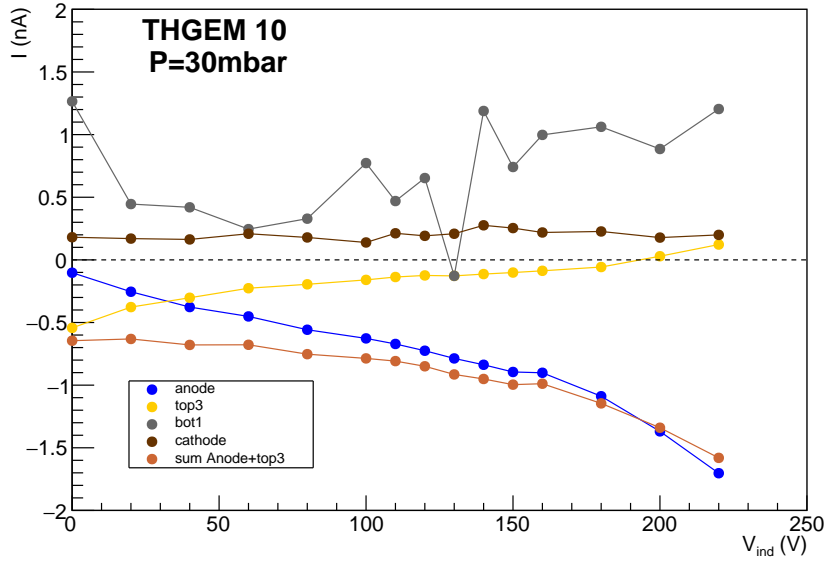
Table 2.1: The values of pressure (P),  $\Delta V_{TH}$  and  $\Delta V_{drift}$  adopted for the study on  $\Delta V_{ind}$ .

a more evident effect.). For values of  $\Delta V_{ind}$  still higher, the top3 current becomes positive (see Fig. 2.4 b)). That is, a fraction of the positive ions produced in the induction region is cannot flow through the THGEM holes instead is directly collected by the top3 electrode.

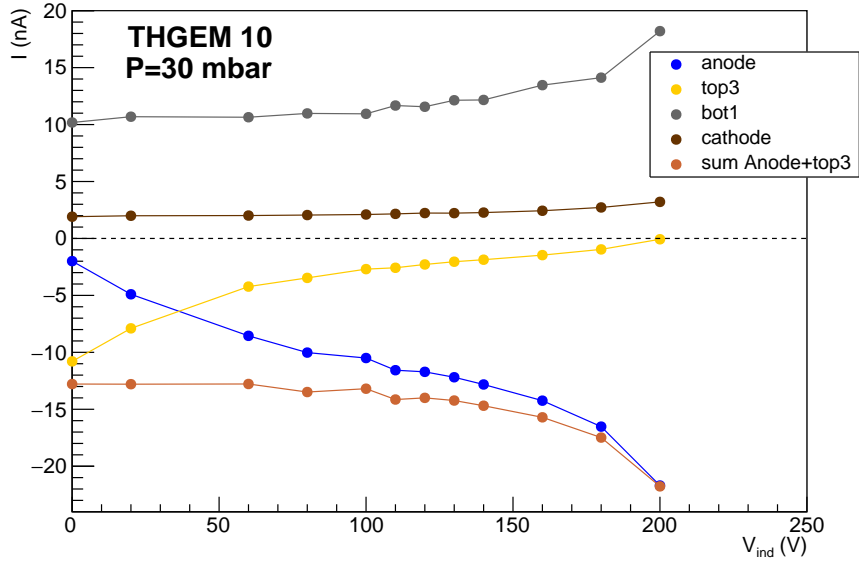
An operational value of  $\Delta V_{ind}=120$  V have been choosen, this value ensure that a large fraction of the electron is collected on the anode and that the multiplication is mainly confined on the THGEM holes.

The scan was repeated for two different values of  $\Delta V_{TH}$ : namely 200 and 230 V (see Fig 2.2) and for two different pressures 10 and 20 mbar Fig. 2.4.

A comparison of anode and top3 current at three different pressures are shown in Fig. ??.

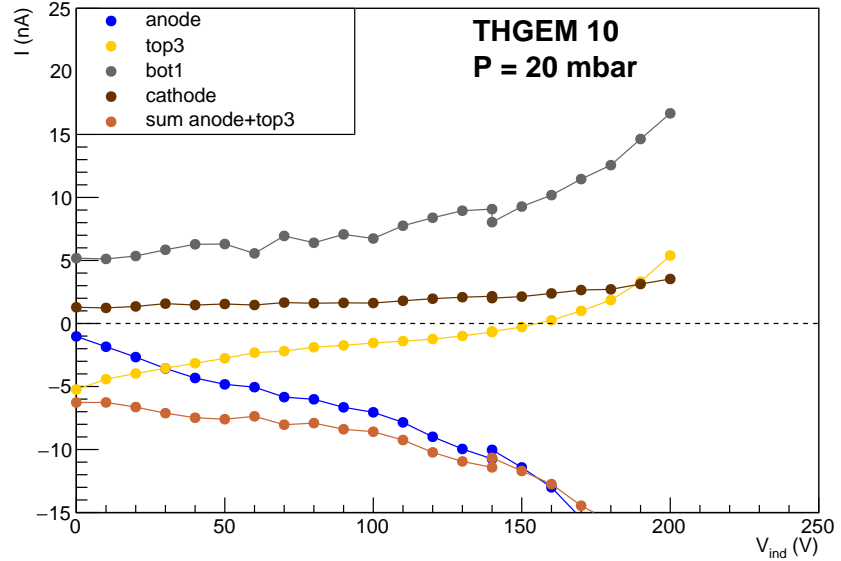


(a)

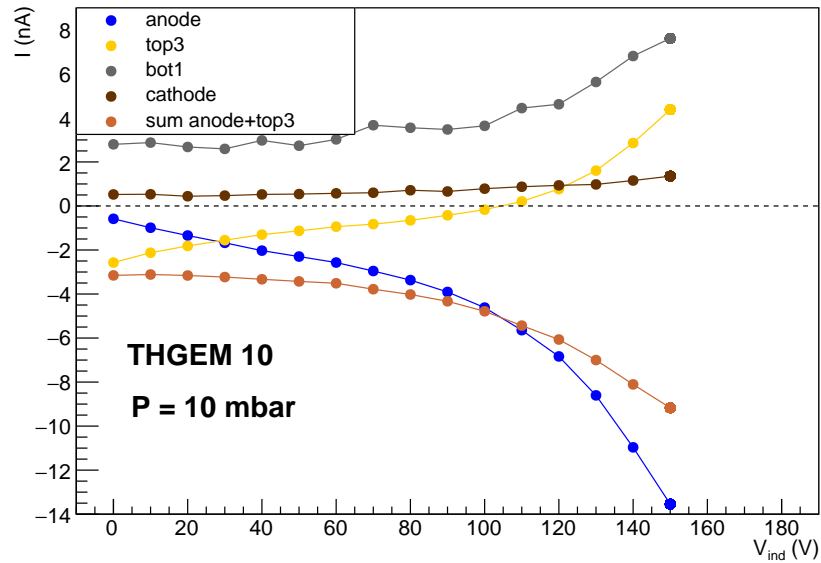


(b)

Figure 2.2: Currents measured during the scan on the voltage  $\Delta V_{ind}$  across the induction region at 30 mbar: in (a) for  $\Delta V_{TH} = 200$  V, in (b) for  $\Delta V_{TH} = 230$  V. In a) the bot1 current fluctuations are due to the lower accuracy of the corresponding PICO channel.



(a)



(b)

Figure 2.3: Currents measured during the scan on the voltage  $\Delta V_{ind}$  across the induction region: in (a) at 20 mbar, in (b) at 11 mbar.

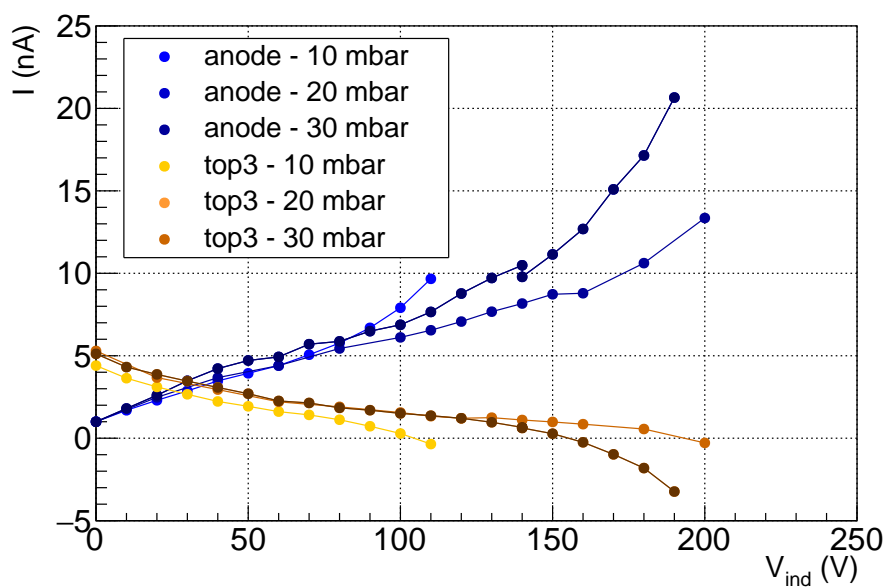


Figure 2.4: Comparison of the anode and top3 currents at pressure of 10, 20, 30 mbar.

### Scan on $\Delta V_{TH}$

In this section the scan of  $\Delta V_{TH}$  are shown. The the  $\Delta V_{ind}$  and  $\Delta V_{drift}$  values were kept fix while the  $\Delta V_{TH}$  was ranging from 0 to a maximum value, corresponding to the discharge, at step of 5/10 V. Table 2.2 shows a scheme of the configurations explored in the scans. Figure 2.5, 2.6(a) and

P (mbar)	$\Delta V_{ind}$ (V)	$\Delta V_{drift}$ (V)	$\Delta V_{TH}$ (V)	run
30	120	1000	180÷235	29-39
20	100	1000	150÷215	112-123
11	70	600	130÷210	169-183
9.3	50	400		440-444

Table 2.2: P,  $\Delta V_{ind}$ ,  $\Delta V_{drift}$  and the explored  $\Delta V_{TH}$  range used in the  $\Delta V_{TH}$  scans.

2.6(b) show the currents vs  $\Delta V_{TH}$  plot for pressure of 30 20 and 10 mbar respectively. A typical exponential trend for increasing  $\Delta V_{TH}$  is evident in all the plot<sup>1</sup>.

From these measurements, the multiplication factors (MFs) were evaluated as a function of  $\Delta V_{TH}$  for different pressures. The MF have been calculated in the following way. Knowing the energy of the incident particles ( $\alpha$  at 5.485 MeV) the pressure of the gas and the length of the track it is possible to calculate the energy lost by  $\alpha$  in the gas. From this, knowing the mean energy for ion-electron pair creation, it is possible to calculate the number of primary electron produced per particle. Knowing the number of  $\alpha$ -particle enetering the detector per second is possible to have an estimate of the total number of primary electron produced per second. From this value and the anodic current is straightforward to get the MF.

The MFs are show n in Figure 2.7, the curves seems to follow an exponential law in good approximation. For a fixed value of  $\Delta V_{TH}$ , the MF decreases with increasing the pressure as expected. The maximum values of the  $\Delta V_{TH}$  reachable depends obviously on the gas pressure but seems not to follow a simple decreasing law.

---

<sup>1</sup>The exponential bheaviour for the anode is confirmed looking at the Multiplication Factor plot in the following.

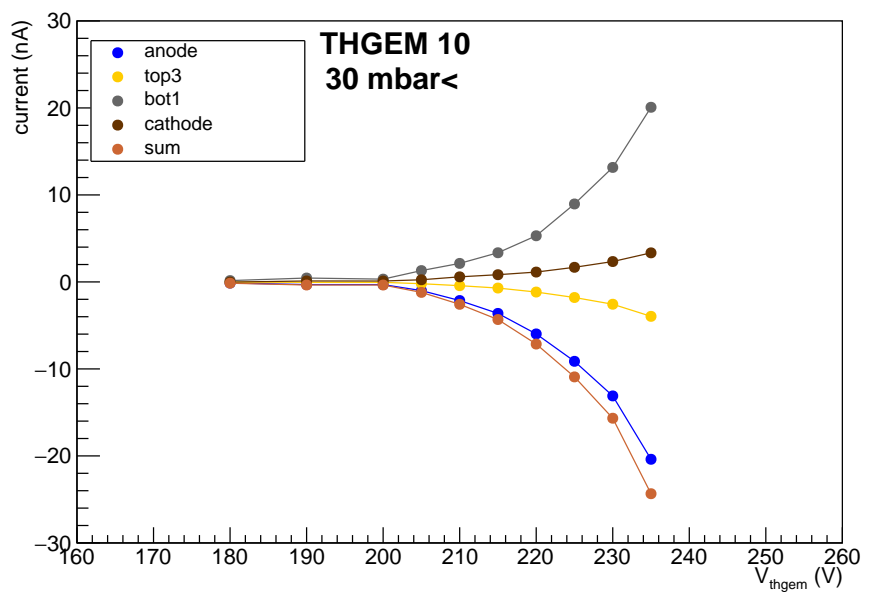
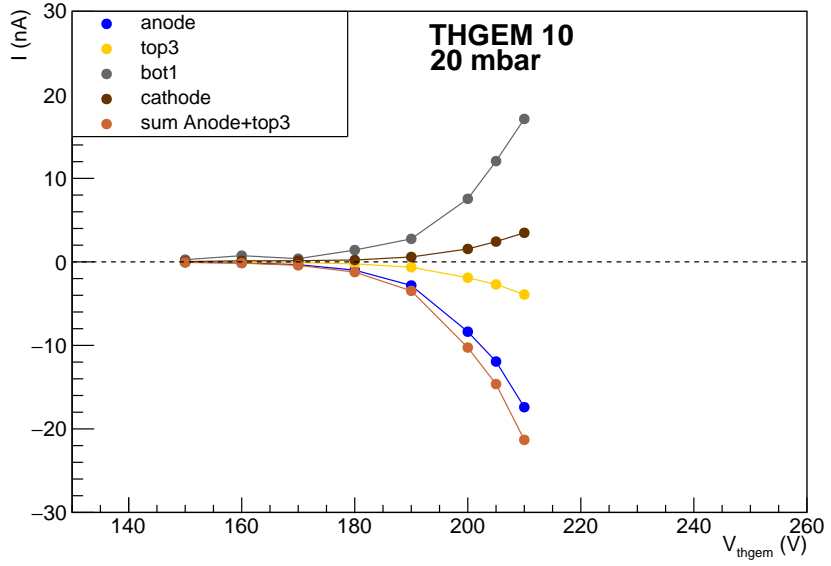
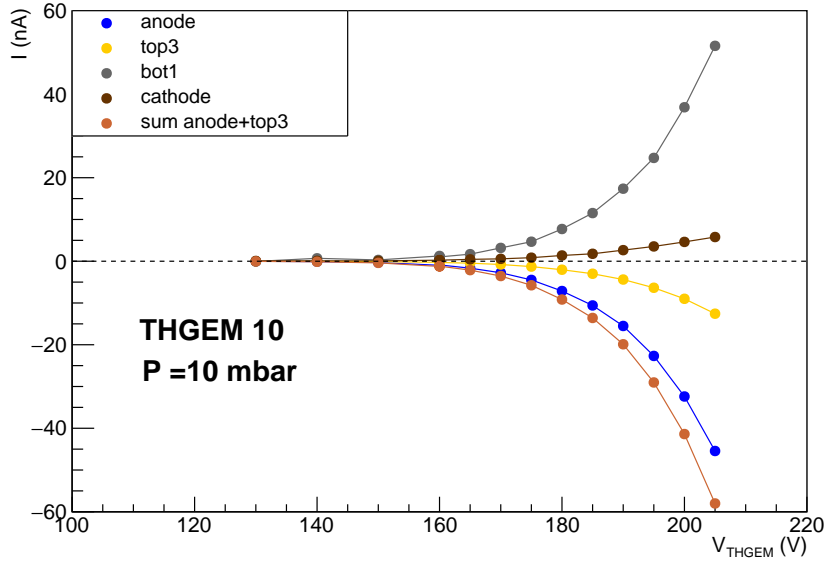


Figure 2.5: Currents measured during the scan on the voltage  $\Delta V_{TH}$  across each FULL THGEM at 30 mbar.



(a)



(b)

Figure 2.6: Currents measured during the scan on the voltage  $\Delta V_{TH}$  across each FULL THGEM: in (a) with  $P = 20$  mbar,  $\Delta V_{ind} = 100$  V and  $\Delta V_{drift} = 1000$  V, in (b) with  $P = 11$  mbar,  $\Delta V_{ind} = 70$  V and  $\Delta V_{drift} = 600$  V.

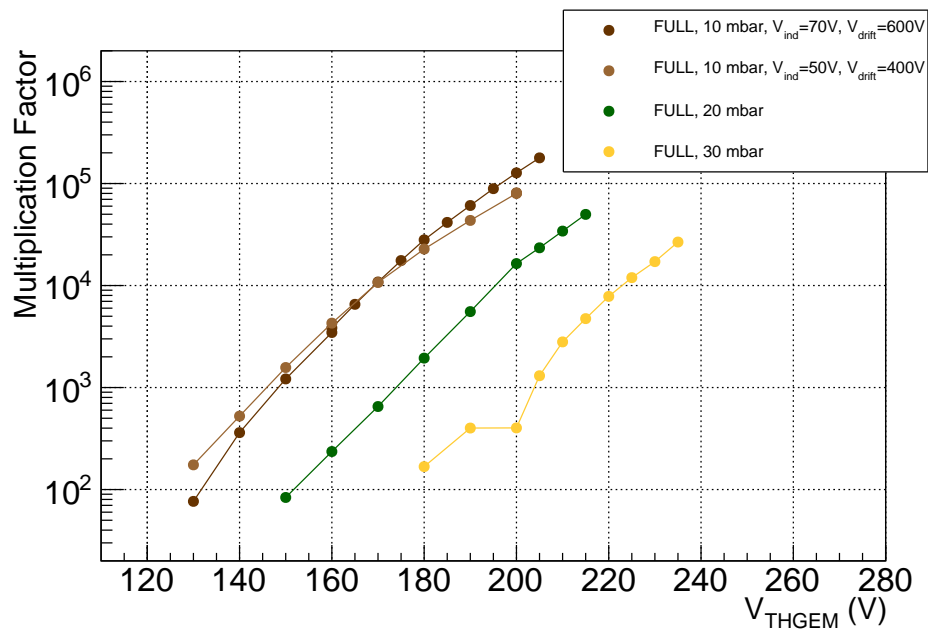


Figure 2.7: The multiplication factors evaluated for the FULL THGEM as a function of  $\Delta V_{TH}$  and pressure.

### Scan on $\Delta V_{drift}$

In this section the behaviour of the prototype as a function of  $\Delta V_{drift}$  have been studied. As in previous case, while pressure,  $\Delta V_{ind}$  and  $\Delta V_{TH}$  were kept fixed,  $\Delta V_{drift}$  was varied from 0 V (or 100 V) to the discharge voltage<sup>2</sup>, which depends on the gas pressure; in fact for  $P = 30$  mbar it was 1600 V, for  $P = 20$  mbar it was 1200 V, and for  $P = 11$  mbar it was 800 V. The  $\Delta V_{drift}$  step was 50 V for  $P = 11$  mbar, and 100 V for the other cases. In Table 2.3 a scheme of the configuration of the prototype is shown.

P (mbar)	$\Delta V_{ind}$ (V)	$\Delta V_{TH}$ (V)	run
30	120	220	40-60
20	100	205	124-138
11	70	190	184-200
11	70	170	201-206
9.3	50	160	440-444

Table 2.3: The values of pressure (P),  $\Delta V_{ind}$  and  $\Delta V_{TH}$  adopted for the study on  $\Delta V_{drift}$ .

The result of the scan at 30 mbar is shown in Figure 2.8.

The anodic current seems not be dependent on the values of the  $\Delta V_{drift}$ . In fact the value of the anodic current is basically constant but for the point at  $\Delta V_{drift}=0$ V where, surprisingly, a value of the anodic current different from zero is observed. For the sake of curiosity further measurements were done to investigate the behaviour of the prototype at very low  $\Delta V_{drift} = 30$  V, 20 V, 20 V, and 5 V. Till so small values<sup>3</sup> the anodic current is still constant and do not decreases, for a magnified view see Figure .

Conclusion are that the  $\Delta V_{drift}$  at so small rate of event do not affects the collection of the primary electron even at very small  $\Delta V_{drift}$ . Concerning the fact that at  $\Delta V_{drift}=0$ V we still see the anodic current we suspect that the PICO picoammeter or the CAEN power supply introduce some very small  $\Delta V_{drift}$  that is enough to collect a large fraction of the primary electron<sup>4</sup>.

In Figure 2.8 the orange line represents, in this case, the sum of the cathode and bot1 currents. This quantity is important to estimate the Ion Backflow (IB).

The scans at 20 and 11 mbar are shown, respectively, in Figure 2.10(a) and 2.10(b). The IB, defined of the ration between the current flowing in the cathode and the TNC that is the sum of current flowing in the anode

---

<sup>2</sup>Discharge is most probably due to the "effetto punta" between conductor elements at the same potential of the cathode with the ground.

<sup>3</sup>for  $\Delta V_{drift}=5$ V the elctric field in the drift region is about  $5/20$  (V/cm) =

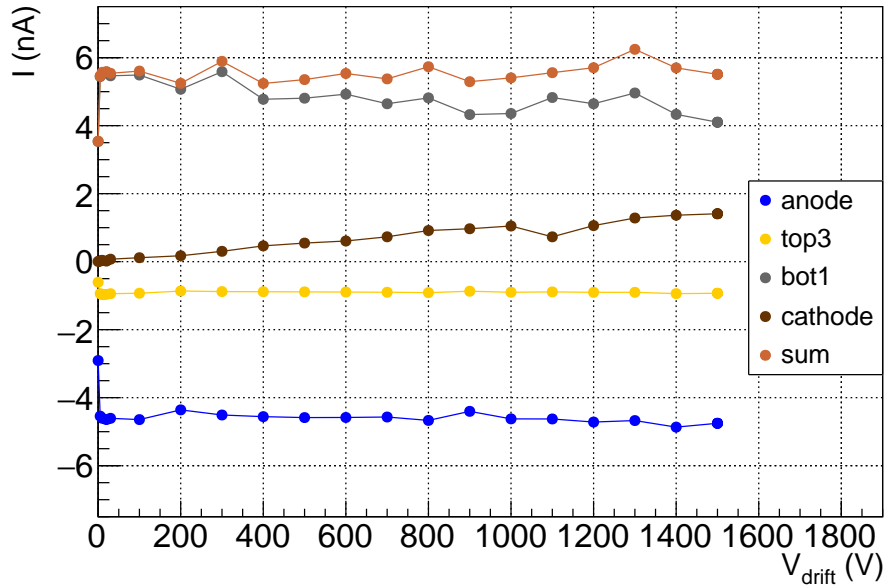


Figure 2.8: Currents measured during the scan on the voltage  $\Delta V_{drift}$  across the drift region at 30 mbar.

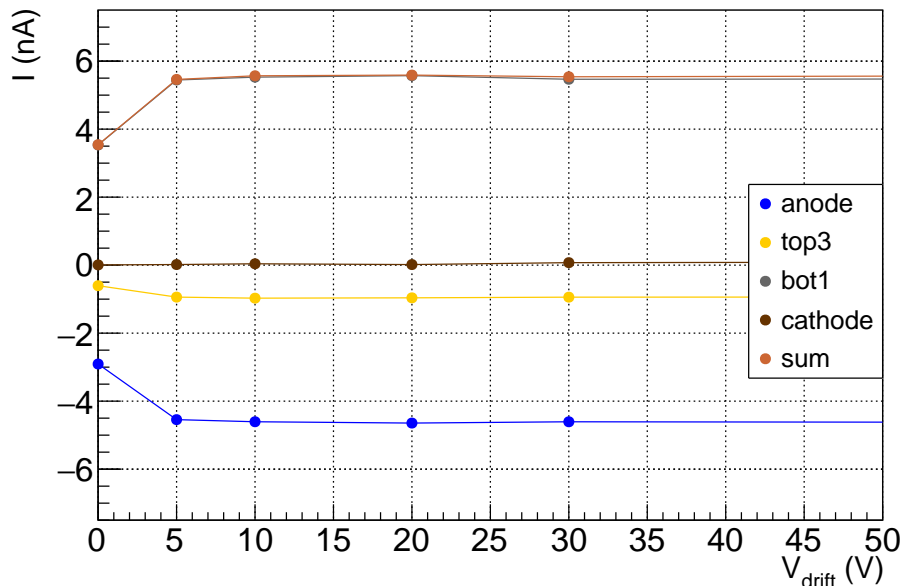
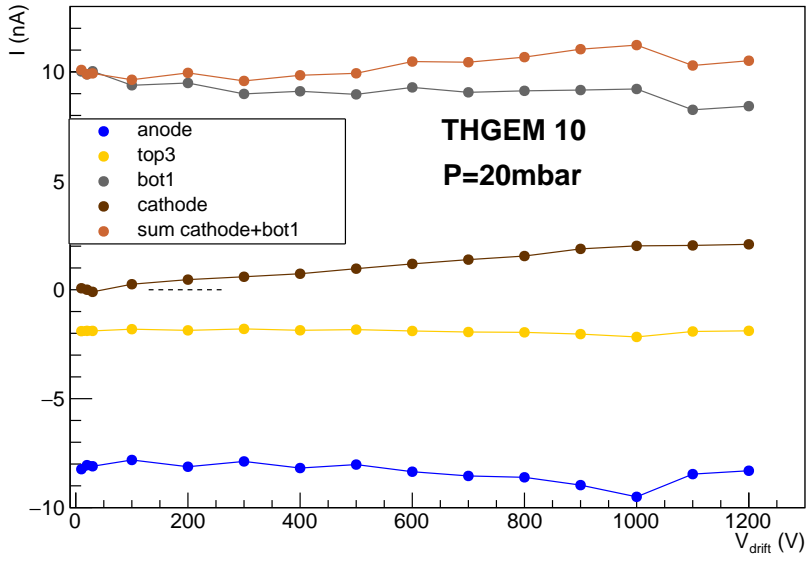
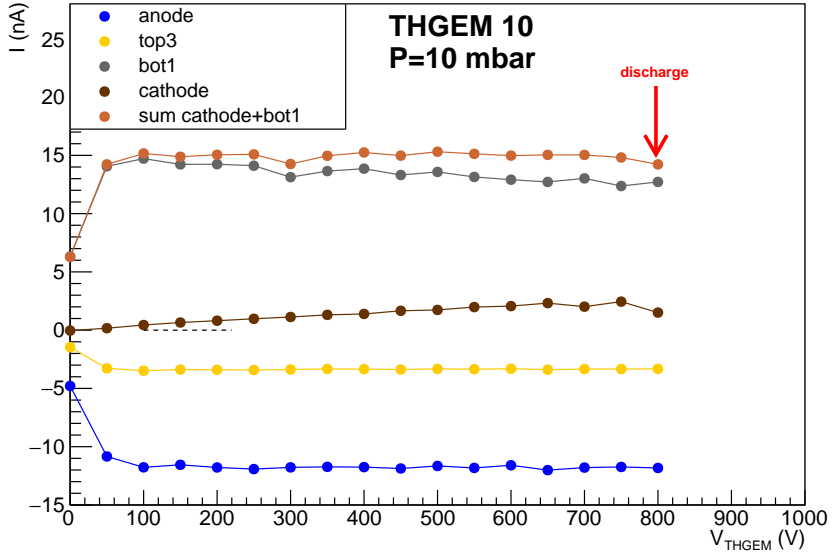


Figure 2.9: Magnification of Fig. 2.8.



(a)



(b)

Figure 2.10: Currents measured during the scan on the voltage  $\Delta V_{drift}$  across the drift region: in (a) at 20 mbar, in (b) at 11 mbar.

250 (mV/cm).

<sup>4</sup>Some simulation could be very useful to understand such phenomena.

and in the top3, have been also plotted as a function of the  $\Delta V_{drift}$ .

In Figure 2.11 is evident the trend of the ion backflow that increases, almost linearly for increasing  $\Delta V_{drift}$ . Its value seems not be depending on the pressure. In Figure 2.12 The IBF for three different pressure is shown as a function of the reduced electric field E/p.

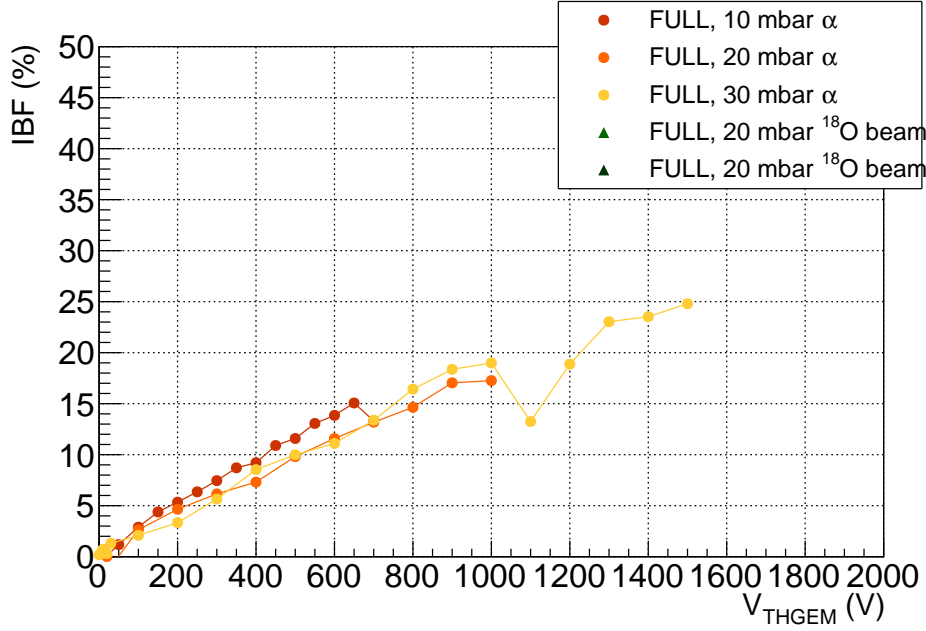


Figure 2.11: The ion backflow as a function of  $\Delta V_{drift}$  for the three examined pressures.

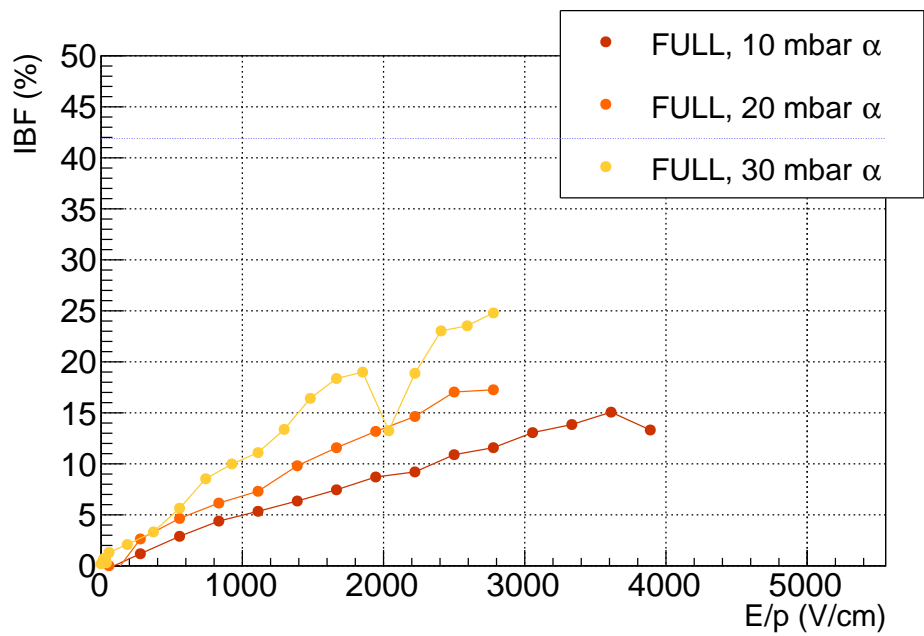


Figure 2.12: As Fig. 2.11 but as a function of the reduced electric field instead of voltage.

### 2.1.2 ROW THGEM

The same studies performed on the FULL THGEM have been repeated on the ROW THGEM. We shortly recall that the main difference respect to the FULL THGEM is the significantly lower number of holes. Therefore we expect that, for similar condition, the currents on the ROW THGEM are smaller compared to those of the FULL THGEM. Moreover this make difficult to estimate the MF since we do not know the actual number of primary electrons that reach the multiplication stage (the holes). In fact, part of the electron reach the no-hole region and therefore are not multiplied while an unknown fraction of primary electron is funneled through the holes and therefore multiplied.

#### Scan on $\Delta V_{ind}$

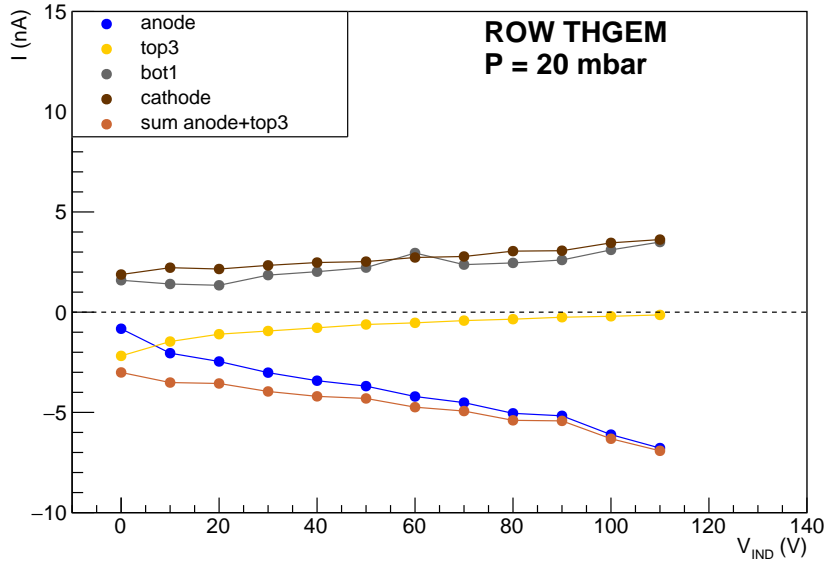
The  $\Delta V_{ind}$  scan have been done fixing pressure,  $\Delta V_{TH}$  and  $\Delta V_{drift}$  and changing the  $\Delta V_{ind}$  at step 10/20 V from 0 V to the discharge value that was 110 V fot  $P = 20,30$  mbar and 180 V at  $P = 40$  mbar. A summary scheme of the configurations used in the test is shown in Table 2.4. The two scans

P (mbar)	$\Delta V_{TH}$ (V)	$\Delta V_{drift}$ (V)	run
20.6	220	800	207-218
20.1	210	800	364-378
30	240	800	233-244
42	260	700	283-299

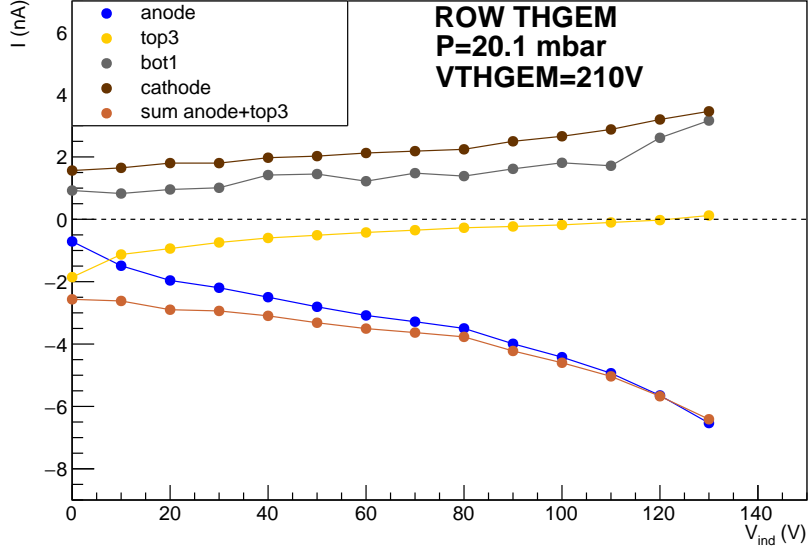
Table 2.4: The values of pressure (P),  $\Delta V_{TH}$  and  $\Delta V_{drift}$  adopted for the study of  $\Delta V_{ind}$ on ROW THGEM.

at 20 mbar are shown in Figure 2.13(a) and 2.13(b). The ROW THGEM behaviour is similar to that of the Full THGEM: i.e. raising the value of  $\Delta V_{ind}$ , the anodic current (blue line) increases, while the top3 current (yellow line) approaches to zero. One difference respect to the Full THGEM is that the orange curve (TNC) here is slowly growing, while for the full THGEM there was a region where it was constant (a plateau) and after a given value of  $\Delta V_{ind}$  started to grow. Anyway since the TNC is growing for increasing value of  $\Delta V_{ind}$ , the expansion of the multiplication region out of the THGEM holes is most probably occurring also for the ROW THGEM. Little discharges were observed up to 50 V, while in the range 60÷110 V big discharges affected bot1 and top3 currents. or the Row THGEM at 20 mbar we choose as operational value 50 V or 60 V.

The plot at 30 and 40 mbar are shown in Figure 2.14(a) and 2.14(b), we choose operational values of  $\Delta V_{ind} = 90$  and 60 respectively.

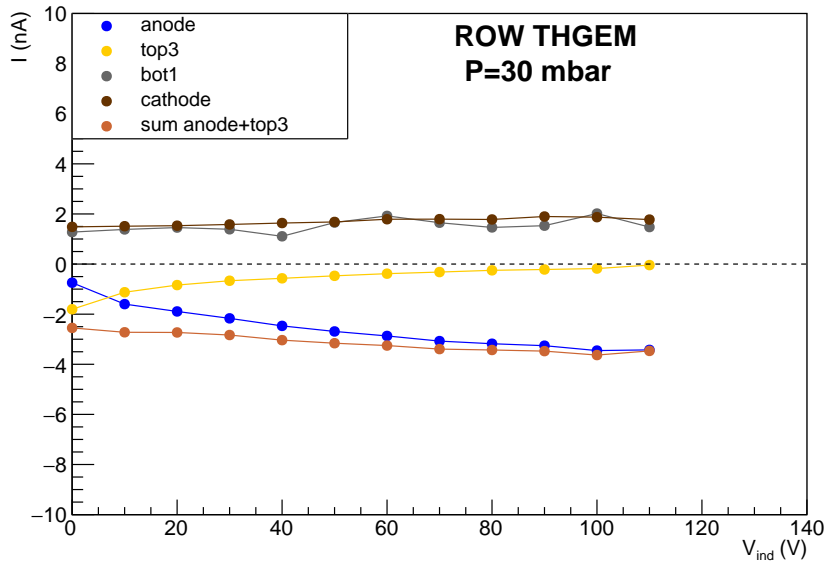


(a)

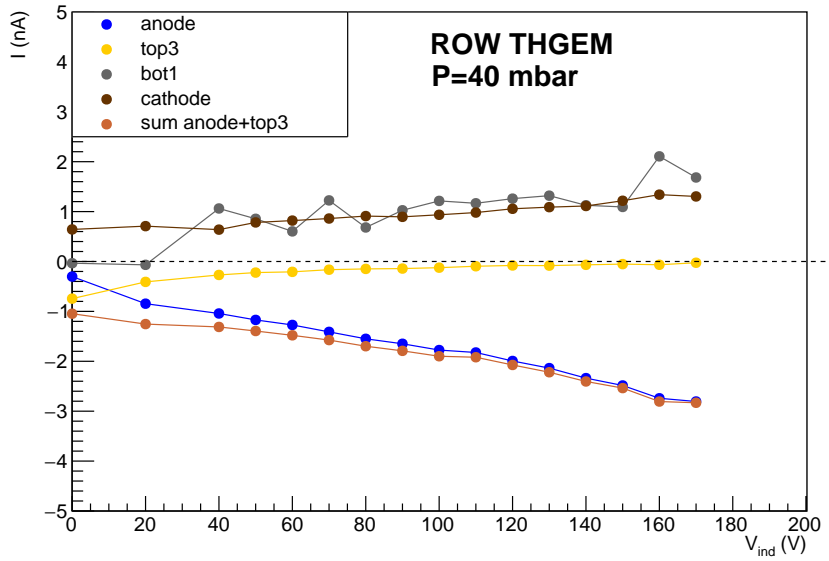


(b)

Figure 2.13: Currents measured during the scan on the voltage  $\Delta V_{ind}$  across the induction region at 20 mbar: in (a)  $\Delta V_{TH}$  is at 220 V, in (b) it is at 210 V.



(a)



(b)

Figure 2.14: Currents measured during the scan on the voltage  $\Delta V_{ind}$  across the induction region: in (a) at 30 mbar, in (b) at 40 mbar.

### Scan on $\Delta V_{TH}$

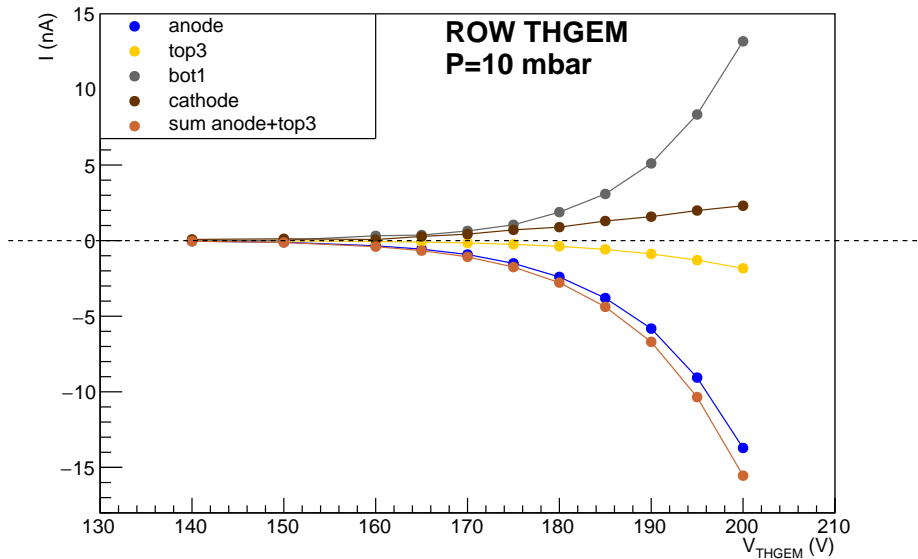
The scan of  $\Delta V_{TH}$  have been done at fixed values of pressure,  $\Delta V_{ind}$  and  $\Delta V_{drift}$  and changing the  $\Delta V_{TH}$  at steps of 5/10 V. A scheme of the different configuration used for the test is shown in Tab. 2.5

P (mbar)	$\Delta V_{ind}$ (V)	$\Delta V_{drift}$ (V)	$\Delta V_{TH}$ range (V)	run
10	50	200	140÷205	342-352
20.6	50	800	180÷225	227-232
21.7	80	300	120÷220	323-341
30	70	800	180÷240	260-267
31.9	70	400	170÷245	309-322
42	80	700	220÷270	300-308

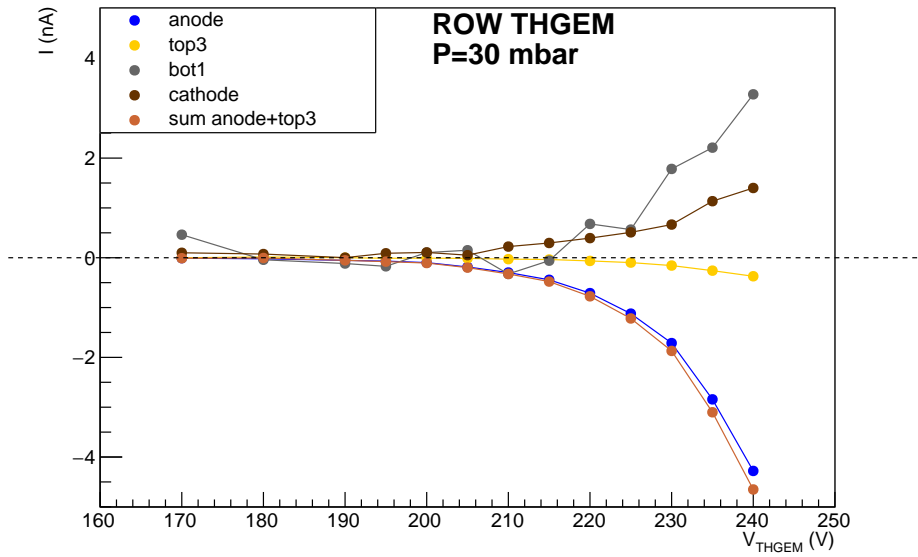
Table 2.5: The values of pressure,  $\Delta V_{ind}$  and  $\Delta V_{drift}$  adopted for the study on  $\Delta V_{TH}$  and the explored  $\Delta V_{TH}$  range.

The scans at 10 and 32 mbar are shown, respectively, in Figure 2.15(a) and 2.15(b): Also in this case the currents follow an exponential law as a function of the increasing  $\Delta V_{TH}$ .

From these measurements, the multiplication factors of the ROW THGEM were evaluated as a function of  $\Delta V_{TH}$  and pressure Fig. 2.16. Some clarification on the way the MF was measured is required. In fact due to the peculiar geometry of the ROW THGEM just a fraction of the primary electrons reach the holes while the remaining fraction of the electrons reach a inert region of the THGEM. Therefore in order to correctly determine the multiplication factor we need to know the fraction of primary electrons that reach the holes. Since we do not know this fraction we assume that it is 1. This assumption has the effect to underestimate the MF. In Fig. 2.17 the comparison of the MF of the two kind of THGEM is shown. As said before it is not possible to make a direct comparison between the two THGEM.



(a)



(b)

Figure 2.15: Currents measured during the scan on the voltage  $\Delta V_{TH}$  across each ROW THGEM: in (a) at 10 mbar, in (b) at 32 mbar.

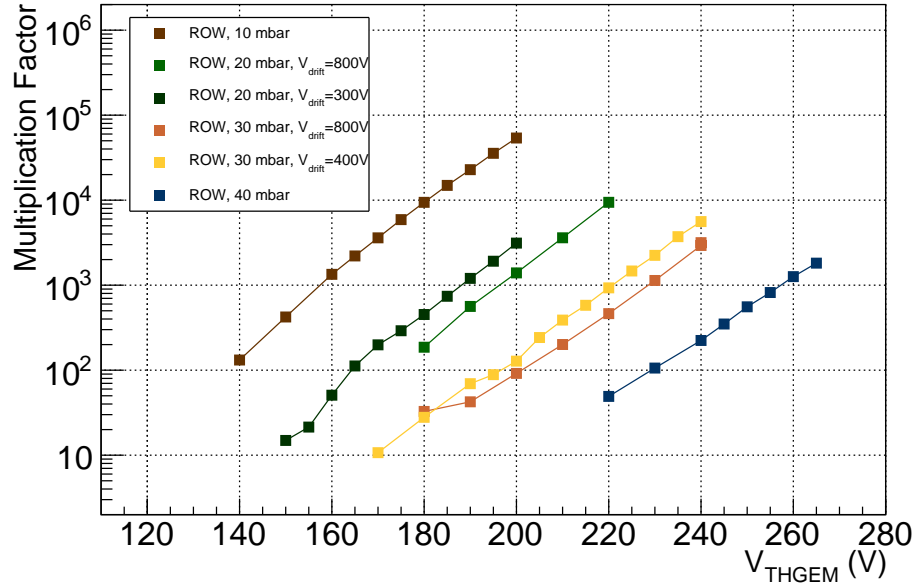


Figure 2.16: Multiplication factors evaluated for the ROW THGEM for different pressures.

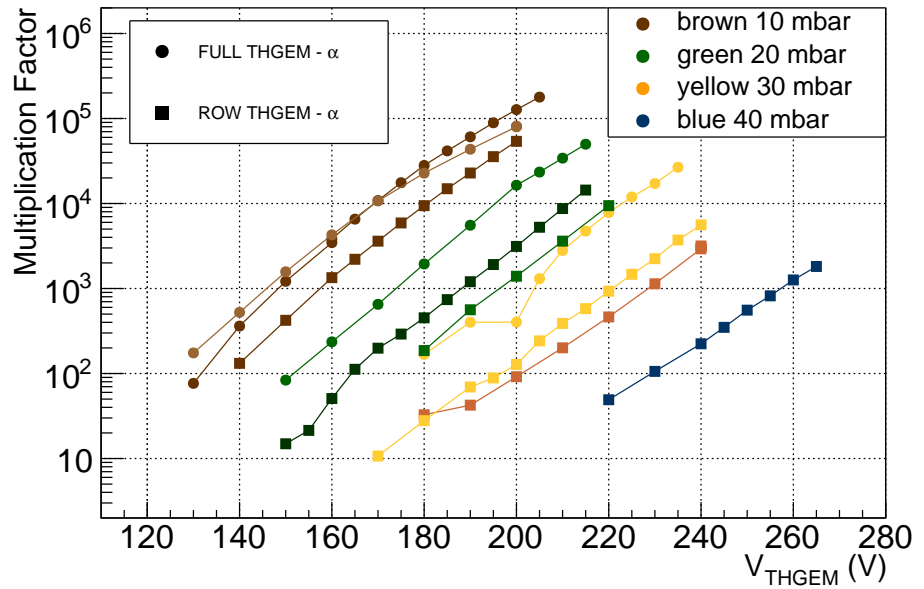


Figure 2.17: Comparison between the multiplication factors evaluated for the ROW THGEM (square) and those for the FULL THGEM (circle) as a function of  $\Delta V_{TH}$  and pressure.

### Scan on $\Delta V_{drift}$

The scan of  $\Delta V_{drift}$  have been done at fixed values of pressure,  $\Delta V_{ind}$  and  $\Delta V_{TH}$ . The explored range goes from 0 V<sup>5</sup> to the discharge voltage. A scheme of the different configuration used for the test is shown in Tab. 2.6

P (mbar)	$\Delta V_{ind}$ (V)	$\Delta V_{TH}$ (V)	$\Delta V_{drift}$	run
30	70	240	0-1400	245-259
30	70	230	0-1400	268-282
20.1	80	210	100-1000	354-363
10	50	180	0-800	379-396

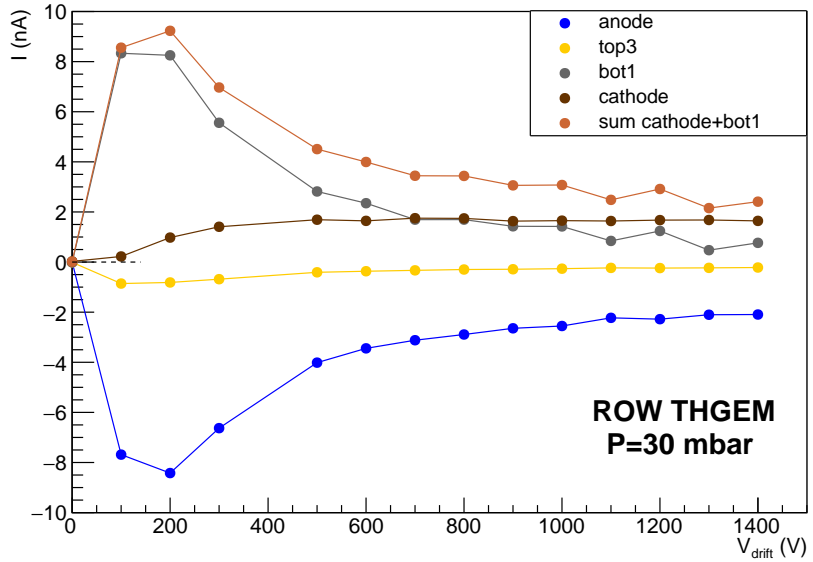
Table 2.6: The values of pressure (P),  $\Delta V_{ind}$  and  $\Delta V_{TH}$  adopted for the study on  $\Delta V_{drift}$ .

The scan of the currents versus  $\Delta V_{drift}$  at 30 mbar are shown in Figure 2.18. The behaviour of the anodic e cathodic current is very peculiar. The currents initially increases<sup>6</sup>, then reach a maximum value and then decrease again reaching a flat region. It is difficult to give a correct explanation of this behaviour without a simulation of the electric field in the prototype. Anyway we can give a tentative and qualitative explanation. It is hardly difficult that this behaviour is due to a change of the multiplication factor of the THGEM since there is no evident reason why it should change so much and with different slopes increasing the  $\Delta V_{drift}$ . Most probably the effect is due to the fact that the change in  $\Delta V_{drift}$ , modify the shape of the electric field in the drift region and therefore change the fraction of the primary electron that reach the holes and are multiplied.

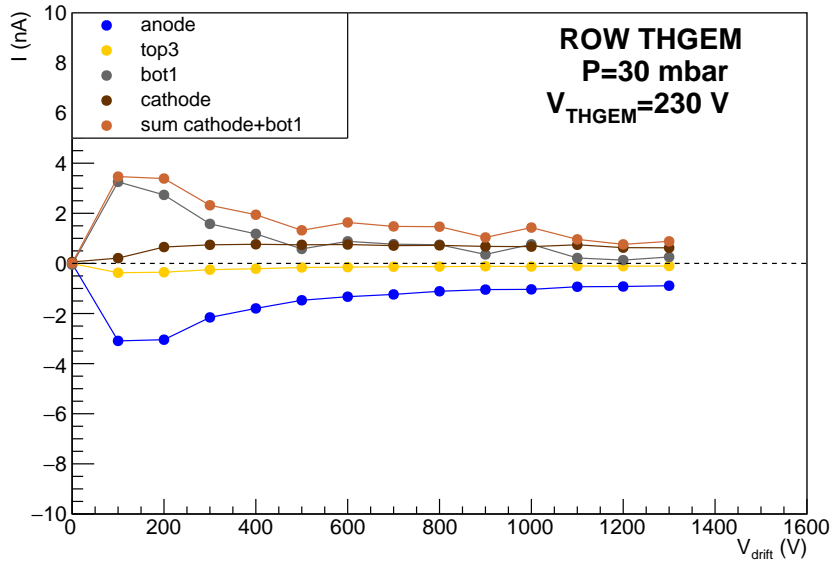
In fact the geometry of the Row THGEM make the electric field in the drift region not homogeneous since part of the field line that start from the cathode will be funneled in the hole while part of them will reach the inert region of the THGEM, i.e. that one without hole. Such ratio is modified by the applied  $\Delta V_{drift}$  therefore affecting the number for primary electron that reach the hole region and are effectively multiplied. The same phenomenon appears also in the scans at 20 and 10 mbar, respectively shown in Figure 2.19(a) and 2.19(b). From these measurements, the ion backflow of the ROW THGEM was evaluated as a function of  $\Delta V_{drift}$  for different pressures. The IBFs are shown in Figure 2.21. In the same figure are shown for comparison also the IBF calculated for the Full THGEM. It is evident that the IBF of the Row THGEM is much higher than that of the Full THGEM reaching values above 70%.

<sup>5</sup>or 100 V in the case with P = 20 mbar

<sup>6</sup>at  $\Delta V_{drift}=0$  they are all 0, that is a different behaviour respect to the Full THGEM.

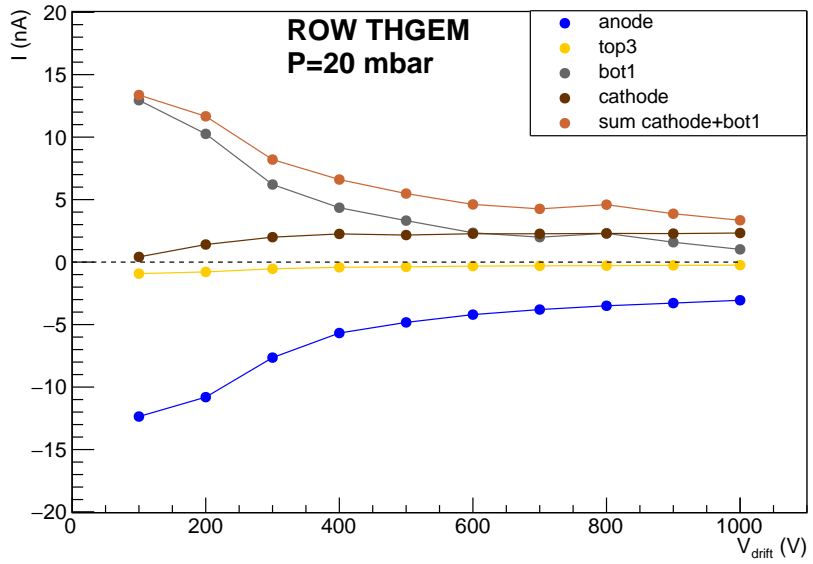


(a)

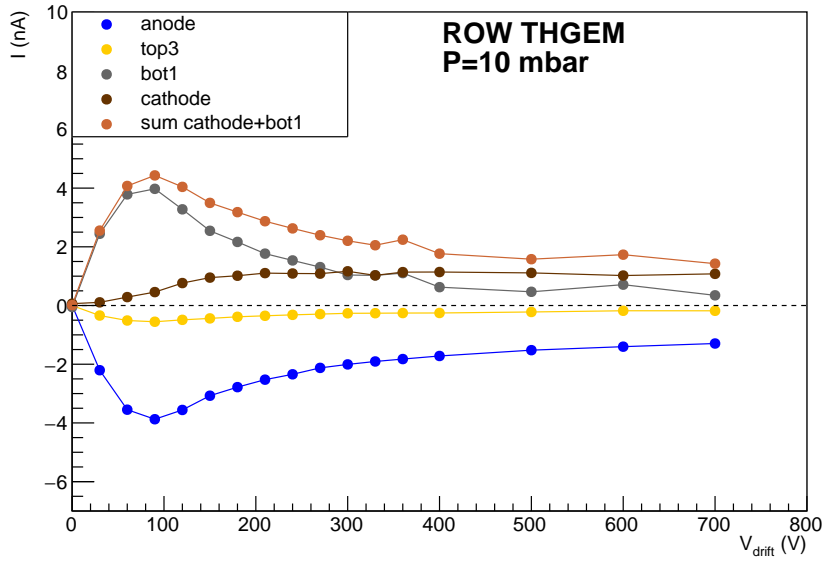


(b)

Figure 2.18: Currents measured during the scan on the voltage  $\Delta V_{drift}$  across the drift region at 20 mbar: in (a)  $\Delta V_{TH}$  is at 240 V, in (b) it is at 230 V.



(a)



(b)

Figure 2.19: Currents measured during the scan on the voltage  $\Delta V_{drift}$  across the drift region: in (a) at 20 mbar, in (b) at 10 mbar.

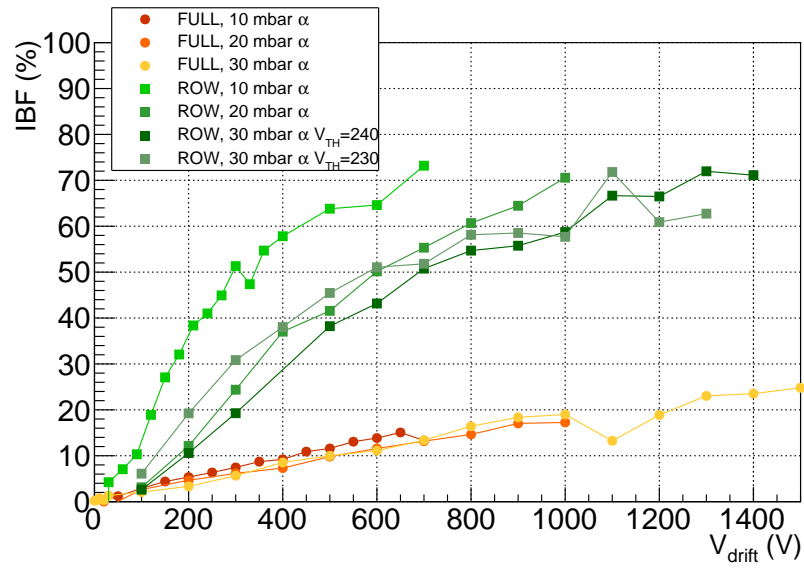


Figure 2.20: Comparison between the ion backflows evaluated for the ROW THGEM (square) and those for the FULL THGEM (circle) as a function of  $\Delta V_{drift}$  for different pressure.

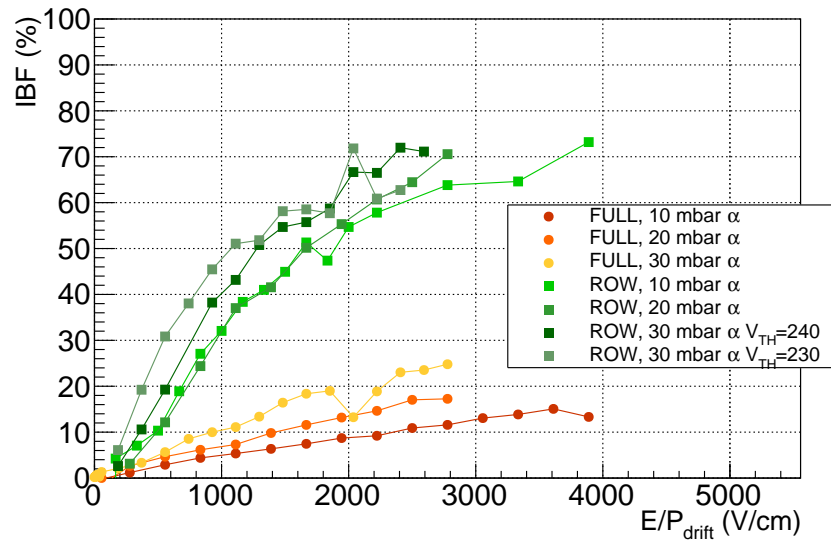


Figure 2.21: Comparison between the ion backflows evaluated for the ROW THGEM (square) and those for the FULL THGEM (circle) as a function of the reduced electric field for different pressure.

**Scan on  $\Delta V_{TH}$**

## 2.2 First test with beam

A first test with beam was performed on 19/02/2020.

A beam of  $^{18}\text{O}$  at an energy of 16.5 AMeV have been sent on a target of  $^{116}\text{Cd}$  xxx  $\mu\text{m}$ . The reaction products enter the scattering chamber housing the prototype that is located at an angle of  $30^\circ$  respect to the beam direction. The pressure of isobutane inside the gas chamber was 9.4 mbar. Since at this energy the elastic cross section for the tracker prototype is not Rutherford It is not possible to know the number and the kind of particles entering the prototype. The only information on the flux comes from the faraday cup FC4 that is placed along the TeBe beam line before the beam line gate valve. Therefore we have relative just relative information that allows to compare run with different beam currents but is not possible to extract absolute information on the particle rate entering the prototype, or make a comparison with  $\alpha$  run.

One possible way to compare such results with the alpha's is to compare directly the anodic current even if it is not fully correct. Being equal all the parameters of the tracker (that is:  $P$ ,  $\Delta V_{TH}$ ,  $\Delta V_{ind}$ ,  $\Delta V_{drift}$ ), it should manifest the same behaviour if the total charge produced is the same, even if the rate of particles entering the tracker is different. In fact even if the same current on the anode can be generate by a very different rates of particles or heavy ions<sup>7</sup> the effects on the tracker are mainly linked to the total amount of charge produced and not on the rate of the particle<sup>8</sup>.

Firstly the tracker was tested at two values of the beam current 60 pA and 400 pA. In order to increase the beam current a collimator was remove from the beam line. In this way we reached much higher values of the beam current: 1, 1.8 nA. Anyway since the optic of the beam is not the same, that is the beam could reach the target with a different emittance, is not correct to compare the first two beam currents with the second two<sup>9</sup>

An important difference respect to the case of the  $\alpha$ -source test is that the rate of the  $\alpha$  particles is constant with a good approximation, the rate of the particle reaching the tracker in the in-beam test is not constant but fluctuate as the beam intensity. The fluctuation occur during the measurements of the currents, that is during the 1-2 minutes during which we take the average of the current and among one measurements and the others. Therefore

---

<sup>7</sup>Ion with different Z, M and energies loose quite different amount of energy...

<sup>8</sup>This is just partially thru. In fact this is valid because we are measuring currents, it is no more if we study the signal on the single strip of the anode. Moreover it is no strictly thru because there is a difference if the total primary charge is produced at very low rate with event that generate a lot of charge ore if the same total charge is produced at very high rate in events where a very small amount of charge is produced

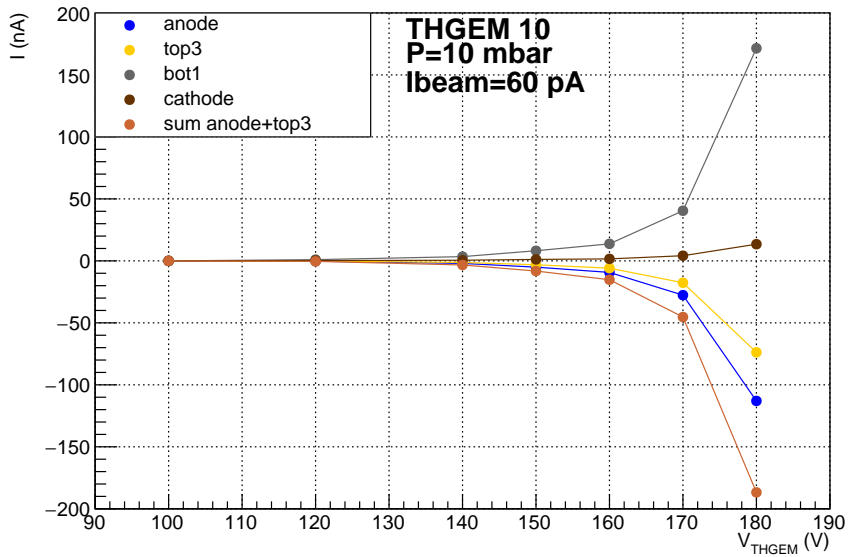
<sup>9</sup>For example if the emittance of the beam was the same we can assert that with a beam of 1 nA we had a rate on the tracker that is 2.5 times ahiger, since the emittance is not the same is not correct to affirm this, moreover also the energy and Z of the particle reaching the tracker could be different.

the plot with beam are less precise and suffers the effect of the fluctuation. Unfortunately such uncertainty are not easy to estimate.

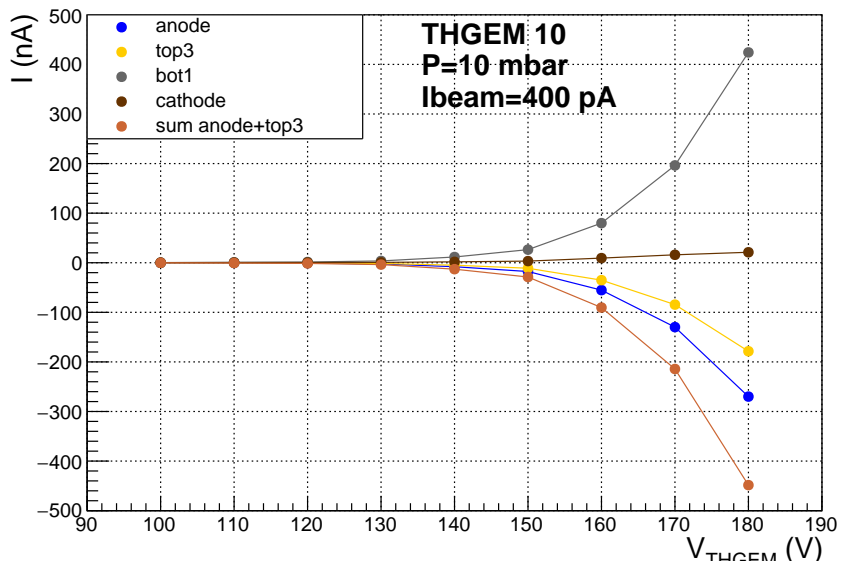
### 2.2.1 Scan on $\Delta V_{TH}$

The measurement was done at  $\Delta V_{ind} = 50$  V and  $\Delta V_{drift} = 400$  V with  $I_{beam}$  60 and 400 pA. The plots of the currents vs  $\Delta V_{TH}$  are shown in Figure 2.22. The plots show have the same behaviour of the scan on  $\Delta V_{TH}$  with  $\alpha$  source (see Figure ??).

The discharge occurred at  $\Delta V_{TH} = 190$  V with both beam intensities, to be compared with  $\Delta V_{TH} = 210$  V for the  $\alpha$  case.



(a)



(b)

Figure 2.22: Currents measured during the scan on the voltage  $\Delta V_{TH}$  across each FULL THGEM fixing  $\Delta V_{ind} = 50$  V and  $\Delta V_{drift} = 400$  V: in (a) at 60 pA, in (b) at 400 pA.

### 2.2.2 Scan on $\Delta V_{drift}$

The measurement was done fixing  $\Delta V_{ind} = 50$  V and  $\Delta V_{TH} = 160$  V. The plots of the currents vs  $\Delta V_{TH}$  are shown in Figure 2.23. The currents have the same behaviour of the scan on  $\Delta V_{drift}$  with  $\alpha$  source (see Figure ??). The discharge voltage was 800 V with both beam intensities to be compared with about 750 V for the  $\alpha$  source. Therefore, apparently there is no difference on the discharge voltage between the two cases  $\alpha$ -spurce, beam.

### 2.2.3 Ion Backflow (IBF)

Figure 2.24 shows the IBF calculations as a function of  $\Delta V_{drift}$  for  $I_{beam}$  equal to 60 and 400 pA. Comparing the two curves we can affirm that there are no significant differences of the IBF for the two beam currents.

Figure 2.25 shows a comparison between the IBFs with  $\alpha$  source and those with beam. IBF as a function of  $\Delta V_{drift}$  seems not sensible to the rate because the curves are basically the same for beam and alpha-source. There are also few points taken at different value of beam currents but at a single value of  $\Delta V_{drift}$ . The trend seems that increasing the beam current and fixing all the other parameters, the IBF decreases. This effect anyway is not so clear and could be simply due to the large uncertainties of the measurements.

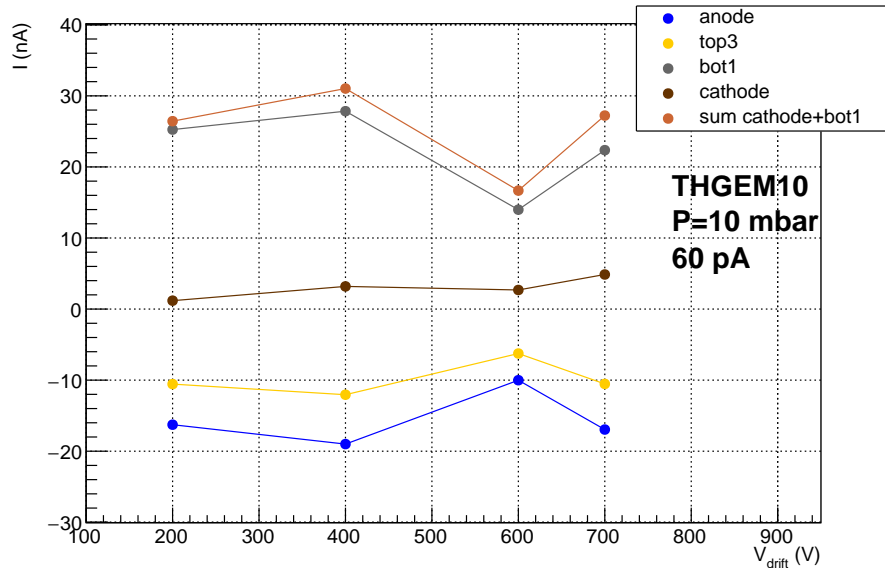
IBF was studied also as a function of  $\Delta V_{TH}$ : the results are shown in Figure 2.26. IBF is nearly constant with varying  $\Delta V_{TH}$ . The best condition to have IBF as less as possible is to work near  $\Delta V_{TH} = 200$  V but as far as possible from discharge.

IBF was studied also as a function of  $\Delta V_{ind}$ : the results are shown in Figure 2.27. As already said, IBF for ROW THGEM is much bigger than that for FULL THGEM. Another difference is that IBF is constant for FULL THGEM and it decreases for ROW THGEM. IBF is not dependent on pressure and it maybe decreases with increasing beam current.

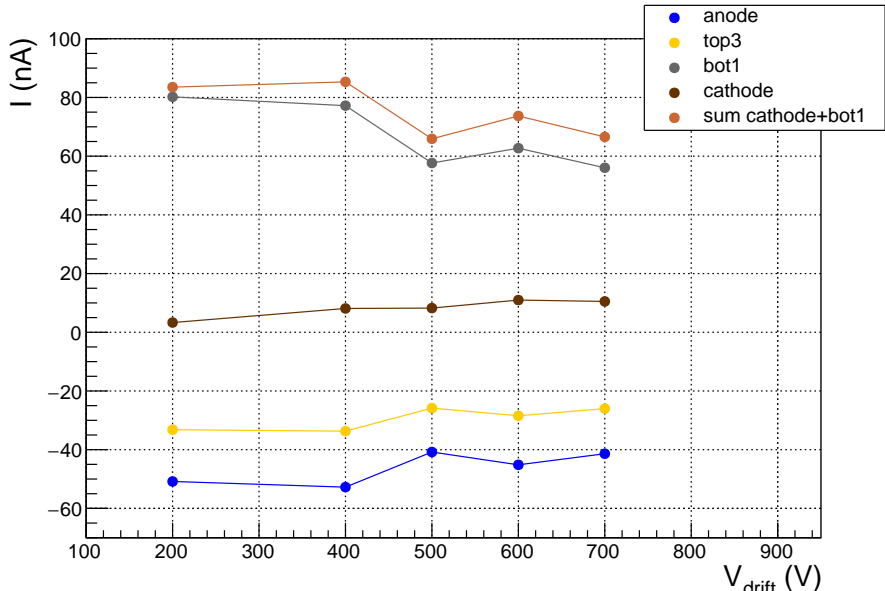
### 2.2.4 Scan on the rate

Ha senso mettere questa parte?

In Figure 2.28 the measured currents were plotted as a function of the beam current ( $I_{beam}$ ). It is important to remember the discussion done at the beginning of the section that is that the points at 1 and 1.8 nA where obtained with a beam that had a different emittance respect to the point at 60 and 400 pA. Therefore the scaling of the rate from the first tow points to the second two is not correct.



(a)



(b)

Figure 2.23: Currents measured during the scan on the voltage  $\Delta V_{drift}$  across each FULL THGEM fixing  $\Delta V_{ind} = 50$  V and  $\Delta V_{TH} = 160$  V: in (a) at 60 pA, in (b) at 400 pA.

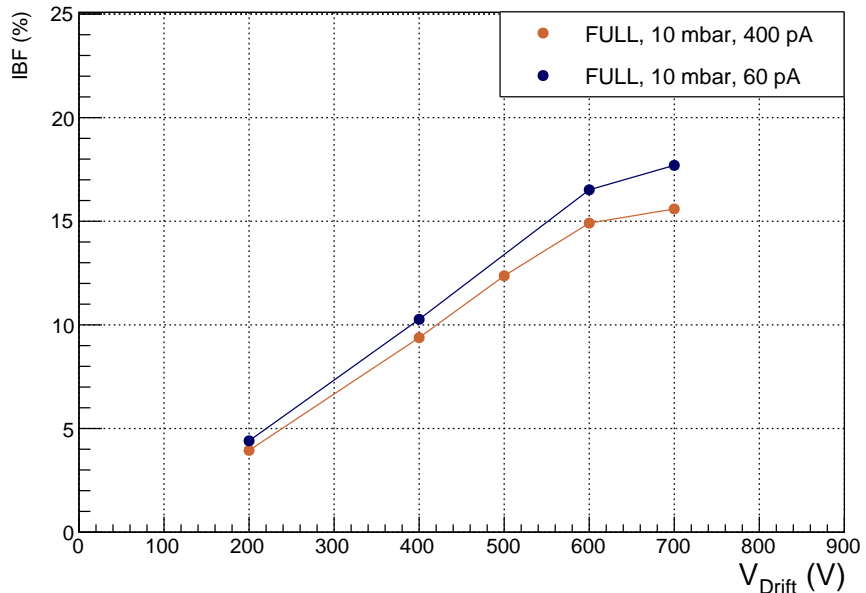


Figure 2.24: Ion backflow evaluated for FULL THGEM as a function of  $\Delta V_{drift}$  at 60 pA and 400 pA fixing  $\Delta V_{ind} = 50$  V and  $\Delta V_{TH} = 160$  V.

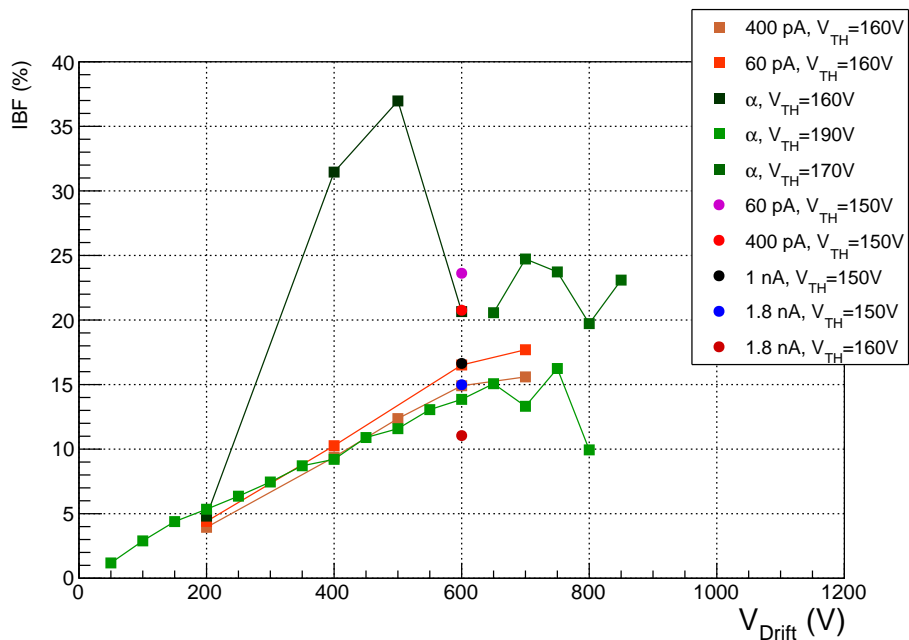


Figure 2.25: Ion backflow evaluated for FULL THGEM as a function of  $\Delta V_{drift}$  at 60 pA, 400 pA, 1 nA, 1.8 nA and with  $\alpha$  source.

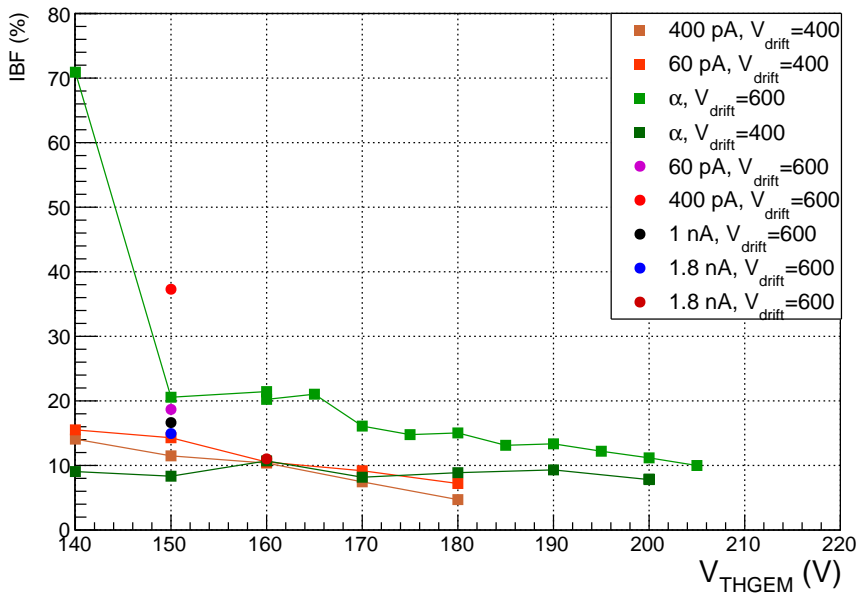


Figure 2.26: Ion backflow evaluated for FULL THGEM as a function of  $\Delta V_{TH}$  at 60 pA, 400 pA, 1 nA, 1.8 and with  $\alpha$  source.

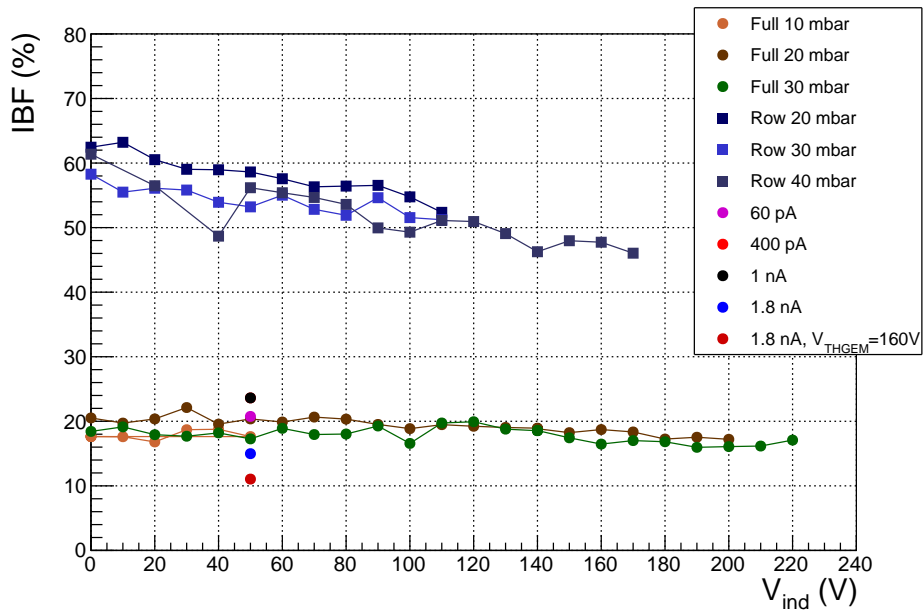


Figure 2.27: Ion backflow evaluated for FULL THGEM as a function of  $\Delta V_{ind}$  at 60 pA, 400 pA, 1 nA, 1.8 nA and with  $\alpha$  source.

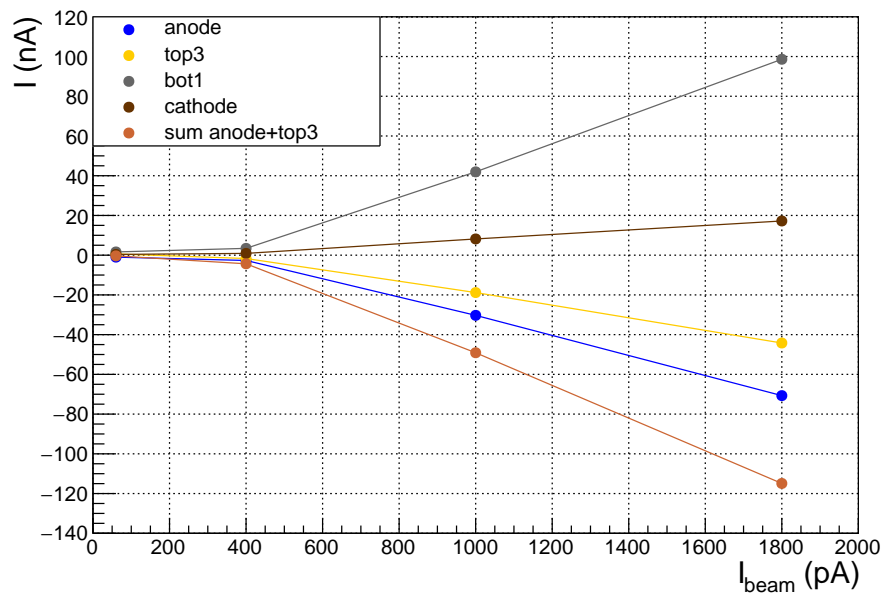


Figure 2.28: Currents measured with varying  $I_{beam}$ .

## 2.3 Second test with beam

The test was performed in march 2020. A beam of  $^{18}\text{O}$  at 145 MeV was sent on two gold targets 0.972 and 9.6 mg/cm<sup>2</sup> thick. The beam intensity was measured by mean of two faraday cups: one upstream the target (MXFC1) and a second downstream the target (TebeFC) that has a lower sensitivity. The tracker prototype is located a 30° respect to the beam direction, at this energy the elastic scattering is Rutherford therefore it is possible to calculate the number of  $^{18}\text{O}$  particles entering the detector. The solid angle<sup>10</sup> of the prototype was about  $6 \cdot 10^{-2}$  sr while the angular range covered is  $30^\circ \pm 6.6^\circ$ . Also a charged particle detector was placed downstream the prototype. It was a silicon photodiode  $1 \times 1\text{cm}^2$  covering a solid angle<sup>11</sup> of  $3 \cdot 10^{-4}$ , while the angular range covered is  $30^\circ \pm 0.47^\circ$ .

The rate of particle entering the prototype was estimated when possible in two independent ways: Assuming Rutherford scattering knowing target thickness and beam current<sup>12</sup>; scaling the counting rate in the photodiode to the solid angle of the tracker prototype.

In Table ?? a scheme of the currents and relative rates used in the test.

---

<sup>10</sup>Distance from the target 470mm and area  $108 \times 120\text{ mm}^2$

<sup>11</sup>Distance from the target 470+130mm

<sup>12</sup>Since, in same case the current read by TBFC2 was below the its sensitivity the faraday cup TBFC1 was used to estimate the current on the target after a scaling.

### 2.3.1 FULL THGEM

#### THGEM scan

The two scans of the  $\Delta V_{TH}$  done at low rate 90 pps and high rate 3400 pps are shown in Fig. 2.29 and 2.30. In Fig. 2.31 a comparison of the

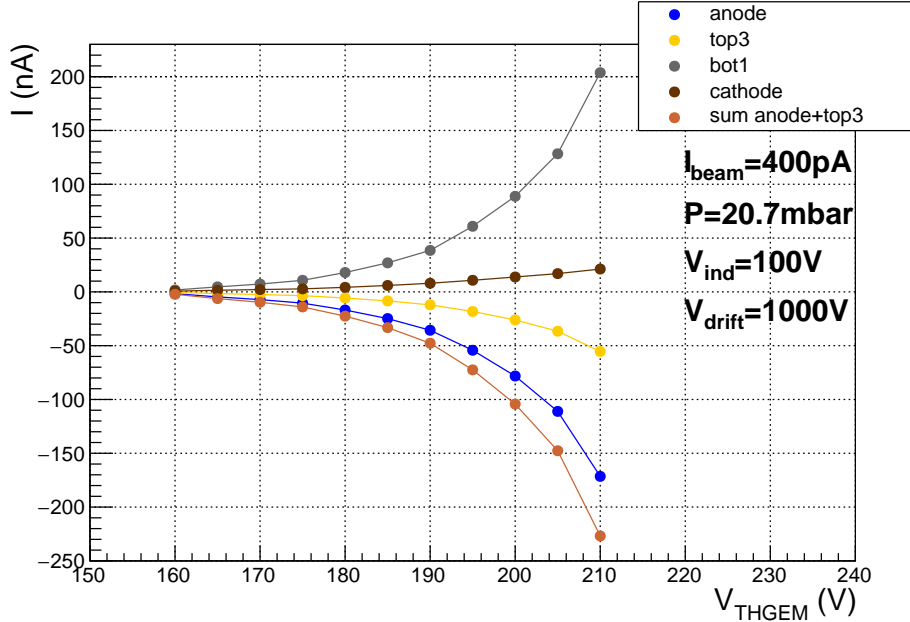


Figure 2.29:  $\Delta V_{TH}$  scan for the highest beam intensity 3400 pps.

multiplication factor as a function of the voltage  $\Delta V_{drift}$  for run with  $\alpha$  source and beam is shown. In Fig. 2.32 same data of Fig. 2.31 but plotted as a function of the reduced electric field of the THEGEM. Some clarification on how the reduced electric field was calculated is necessary. Obviously make no sense to speak about a value of the electric field inside the THGEM since the electric field is not uniform there. We make a very strong approximation that is calculate the electric field as it was uniform that is  $V/d$ .

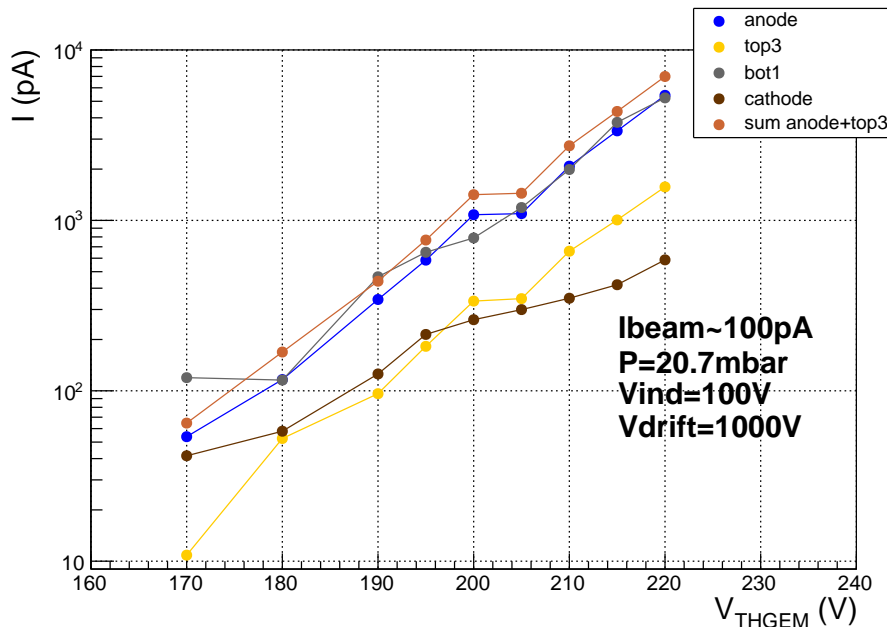


Figure 2.30:  $\Delta V_{TH}$  scan for the lowest beam intensity 87pps.

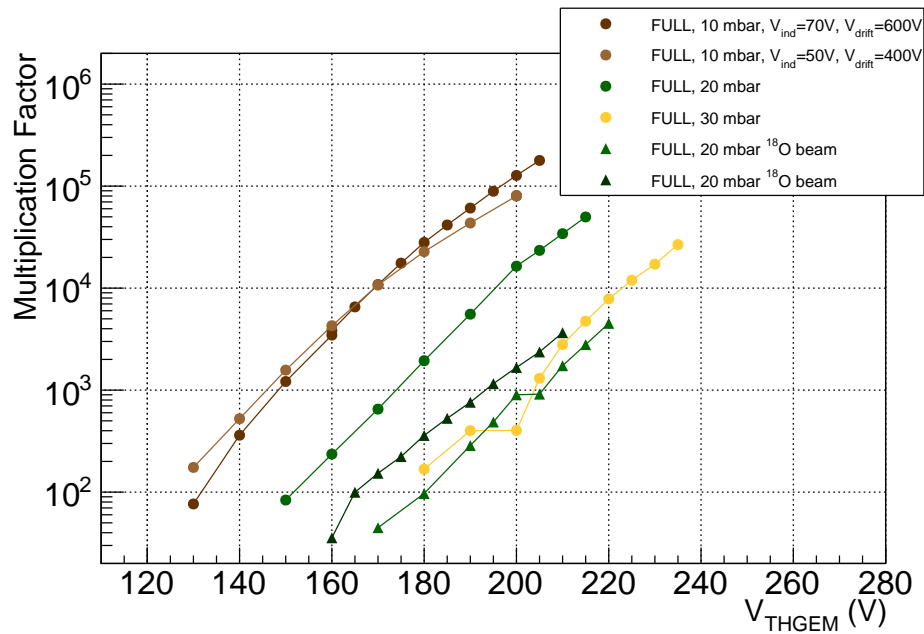


Figure 2.31: MF for the FULL THGEM as a function of the  $\Delta V_{TH}$ . Run with  $\alpha$ -source and  $^{18}\text{O}$  beam are compared.

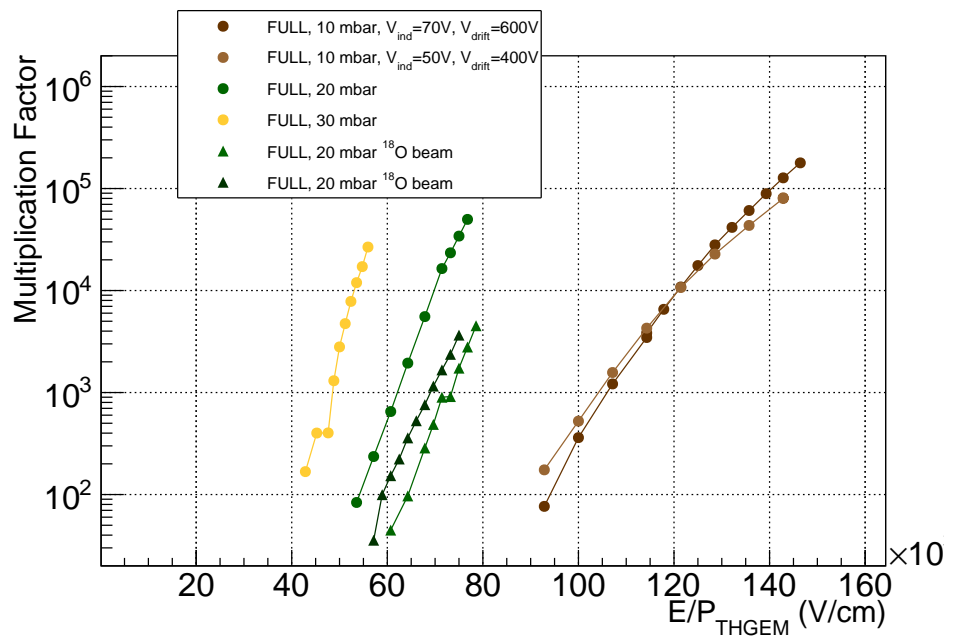


Figure 2.32: MF for the FULL THGEM as a function of the reduced electric field in the THGEM. Run with  $\alpha$ -source and  $^{18}\text{O}$  beam are compared.

## Drift scan

In fig. 2.33 the scan of the  $\Delta V_{drift}$  is shown. No significative difference respect to those obtained with  $\alpha$  are present.

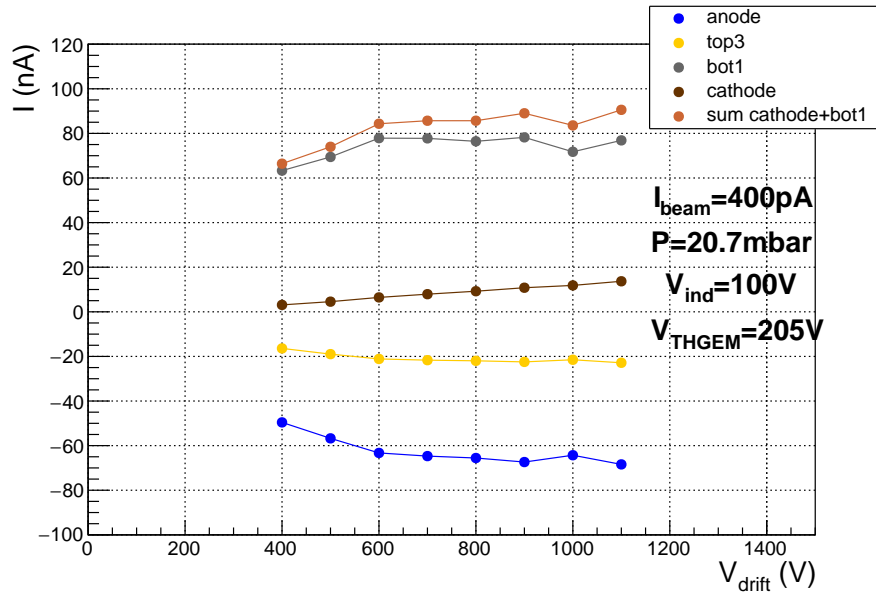


Figure 2.33: IBF for the FULL THGEM as a function of  $\Delta V_{drift}$ . Run with  $\alpha$ -source and  $^{18}\text{O}$  beam are compared.

The ion back flow for the FULL THGEM as a function of the  $\Delta V_{drift}$  and the  $E/p_{drift}$  is shown in Fig. 2.35.

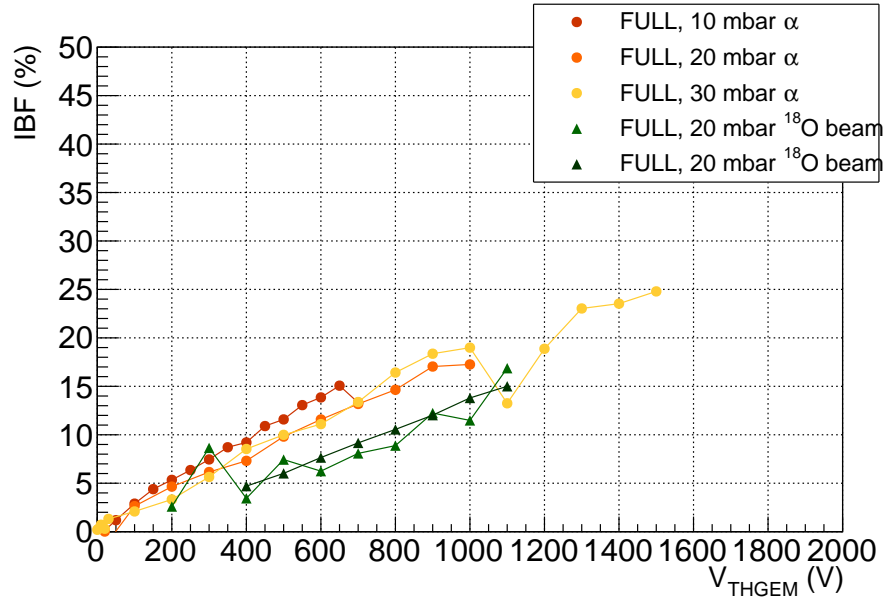


Figure 2.34: IBF for the FULL THGEM as a function of  $\Delta V_{drift}$ . Run with  $\alpha$ -source and  $^{18}\text{O}$  beam are compared.

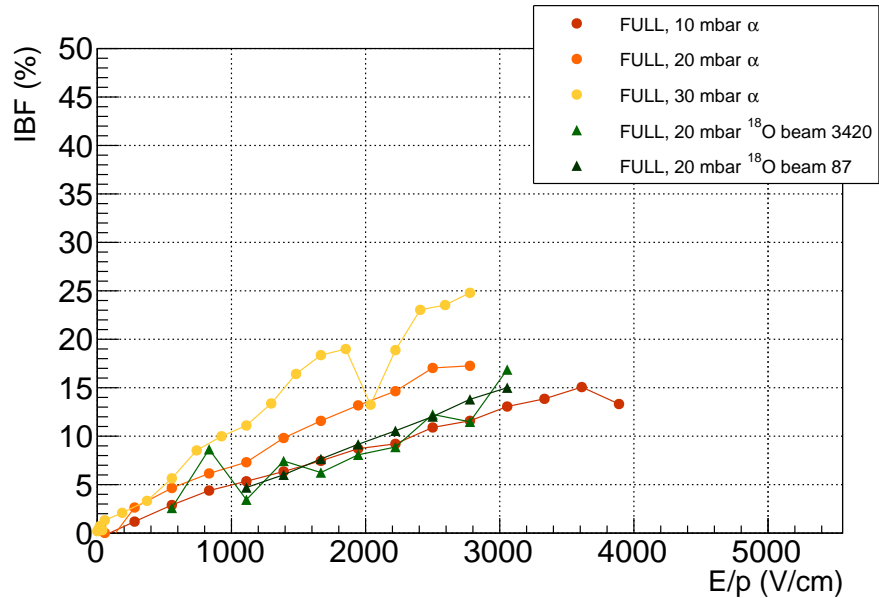


Figure 2.35: IBF for the FULL THGEM as a function of  $E/p_{drift}$ . Run with  $\alpha$ -source and  $^{18}\text{O}$  beam are compared.

## Rate scan

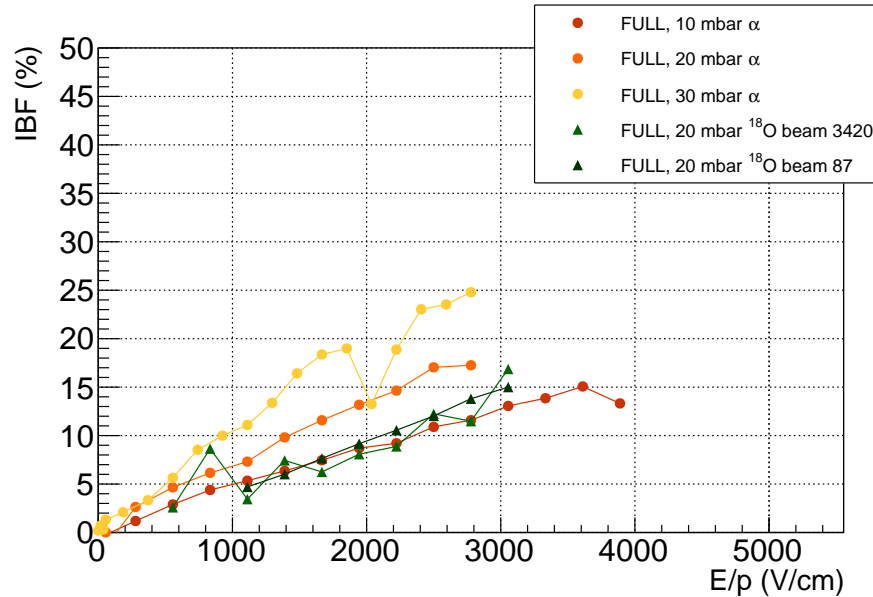


Figure 2.36: Currents measured by Pico for different value of the beam current at  $\Delta V_{drift} =$ .

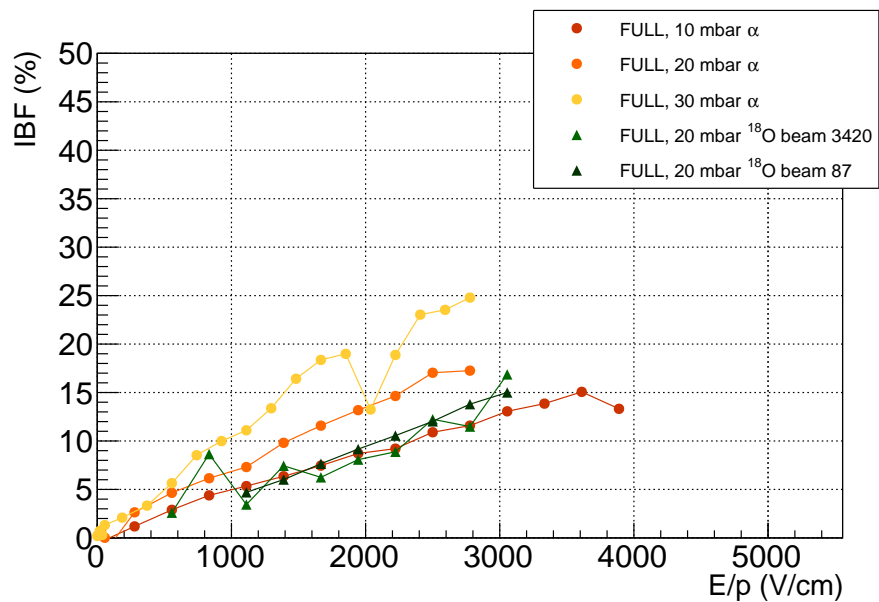


Figure 2.37: Currents measured by Pico for different value of the beam current at  $\Delta V_{drift} =$ .

### 2.3.2 ROW THGEM

#### THGEM scan

The two scans of the  $\Delta V_{TH}$  done at high rate 3400 pps and low rate 130 pps are shown in Fig. 2.38 and 2.39.

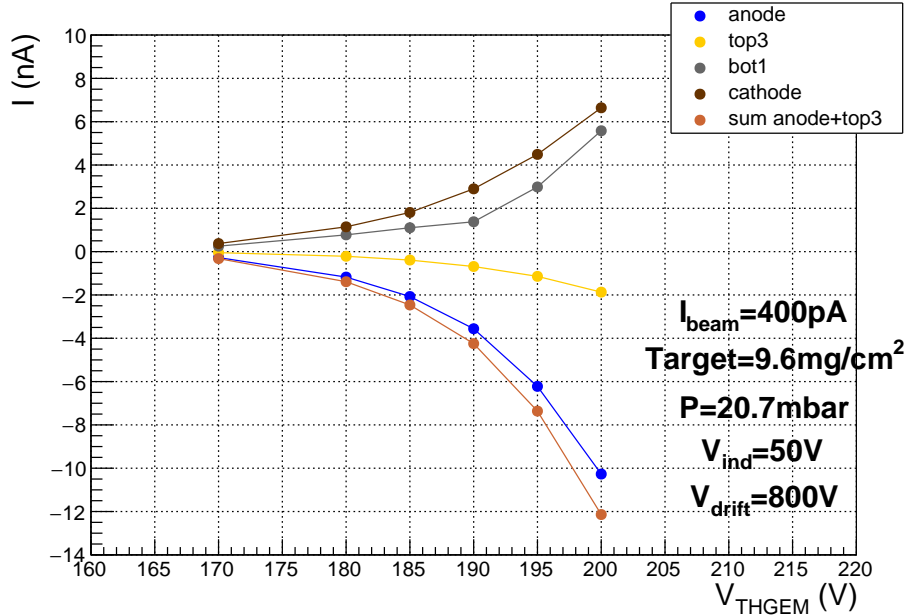


Figure 2.38:  $\Delta V_{TH}$  scan for the highest beam intensity 3400 pps.

In Fig. 2.40 a comparison of the multiplication factors obtained with  $\alpha$  source at different pressures and those with the beam at 20 mbar is shown. Also in this case as for the FULL THGEM there is a mismatch between data with  $\alpha$  source and beam at same values of the pressure.

In Fig. 2.42 A comparison of all the MF for ROW and FULL THGEM including run with  $\alpha$ -source and with beam.

In Fig. 2.40 a comparison of the multiplication factors obtained with  $\alpha$  source at different pressures and those with the beam at 20 mbar is shown. Also in this case as for the FULL THGEM there is a mismatch between data with  $\alpha$  source and beam at same values of the pressure.

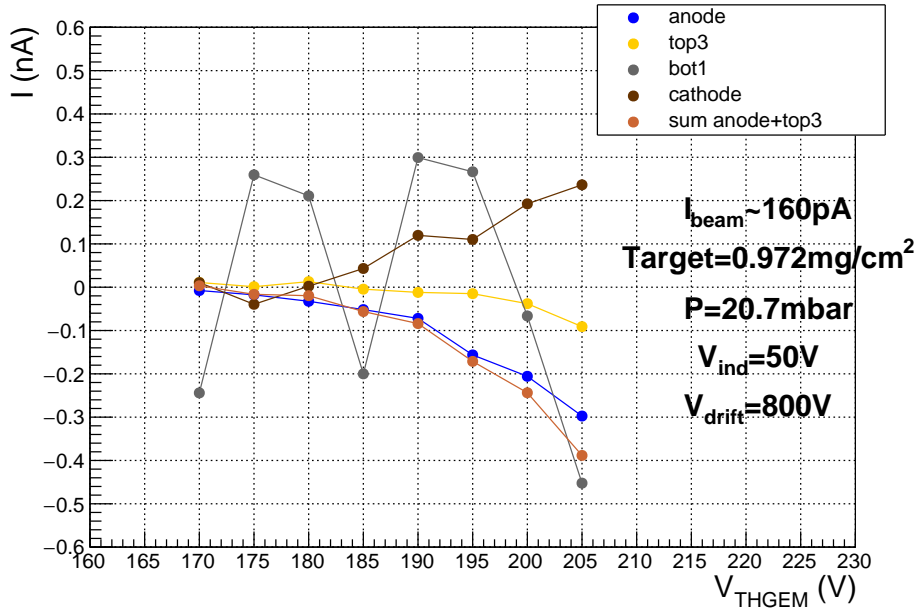


Figure 2.39:  $\Delta V_{TH}$  scan for the lowest beam intensity 130 pps. Bot1 curve is not significative due to the low current measured and the lower accuracy of the bot1 channel.

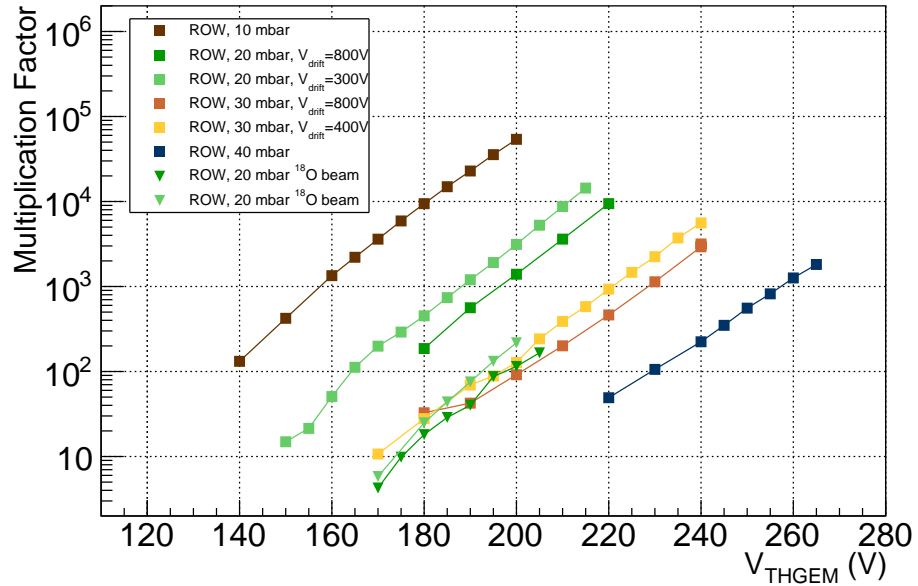


Figure 2.40: MF for the ROW THGEM as a function of the  $\Delta V_{TH}$ . Run with  $\alpha$ -source and  $^{18}\text{O}$  beam are compared.

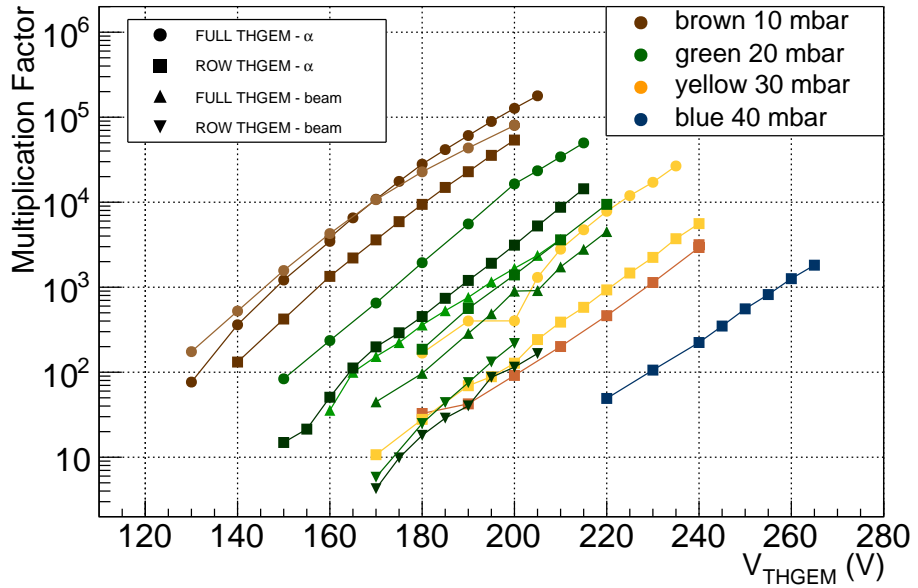


Figure 2.41: MF for the ROW and FULL THGEM as a function of the  $\Delta V_{TH}$ . Run with  $\alpha$ -source and  $^{18}\text{O}$  beam are compared.

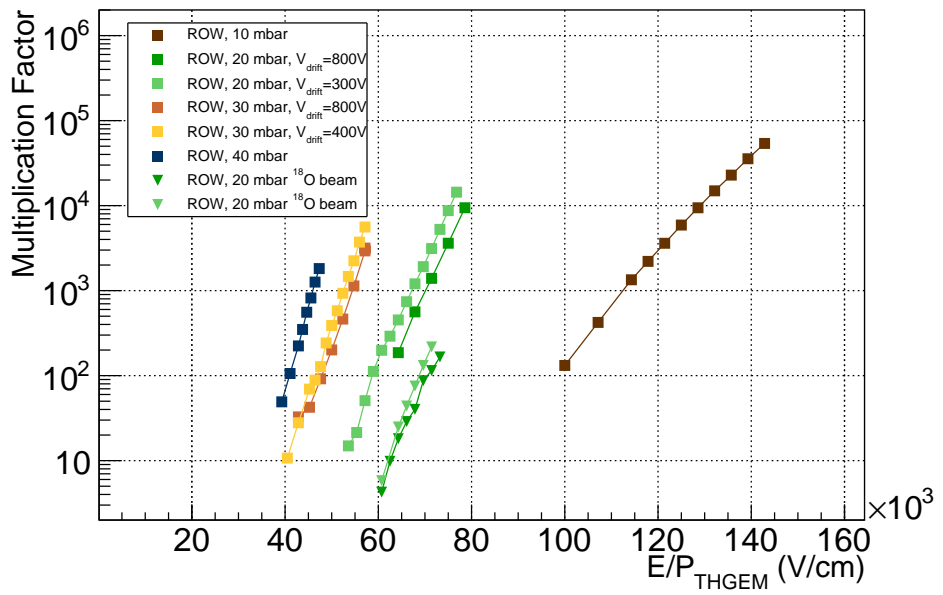


Figure 2.42: MF for the ROW THGEM as a function of the reduced electric field  $\Delta V_{TH}$ . Run with  $\alpha$ -source and  $^{18}\text{O}$  beam are compared.

## Drift scan

In Fig. 2.43 an example of scan of  $\Delta V_{drift}$  with the beam. The behaviour of the curve is similar to that obtained with an  $\alpha$ -source. The anodic current

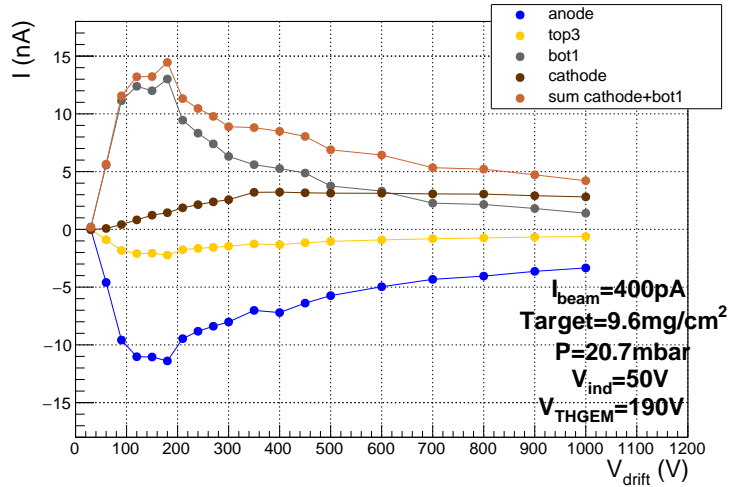


Figure 2.43: Current of the anode as a function of the voltage  $\Delta V_{drift}$  for the ROW THGEM.

of different run done at different conditions is compared in Fig. 2.45. The current are normalized to an arbitrary value. The same quantity is plot as a function of the reduced electric field  $E/p_{drift}$  in Fig. 2.45 in this case the behaviour of the curves is the same for all the run.

In Fig. 2.46 2.47 the IBF is plotted as a function of the  $\Delta V_{drift}$  and  $E/p_{drift}$  respectively.

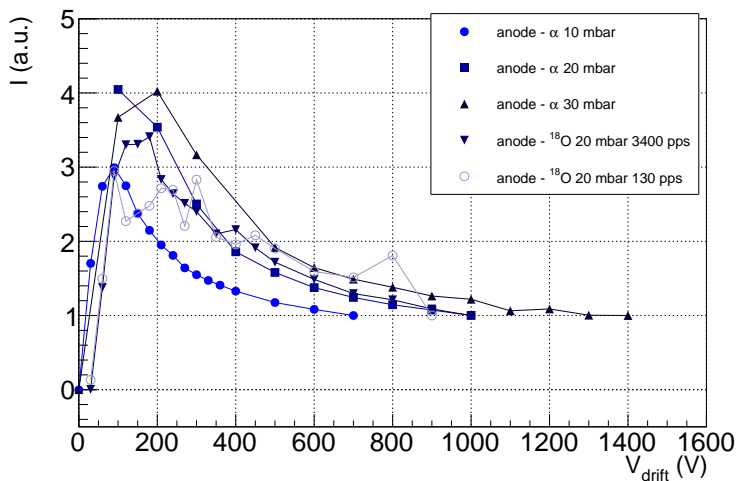


Figure 2.44: Current of the anode (a.u.) as a function of the voltage  $\Delta V_{drift}$  for the ROW THGEM.

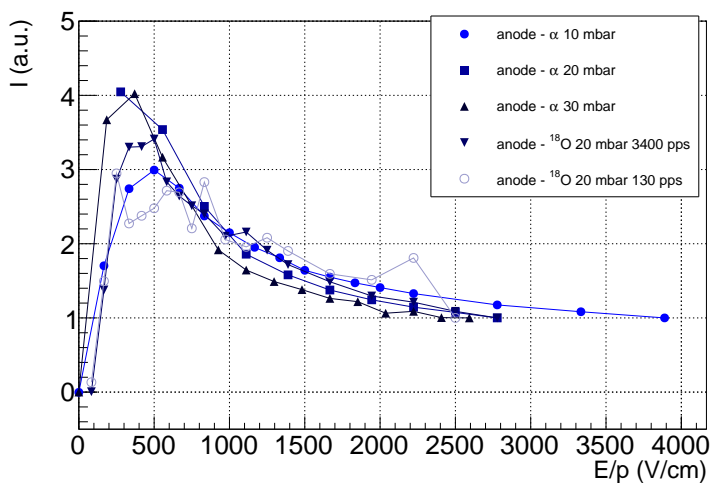


Figure 2.45: Current of the anode as a function of the reduced electric field  $E/p$  for the ROW THGEM.

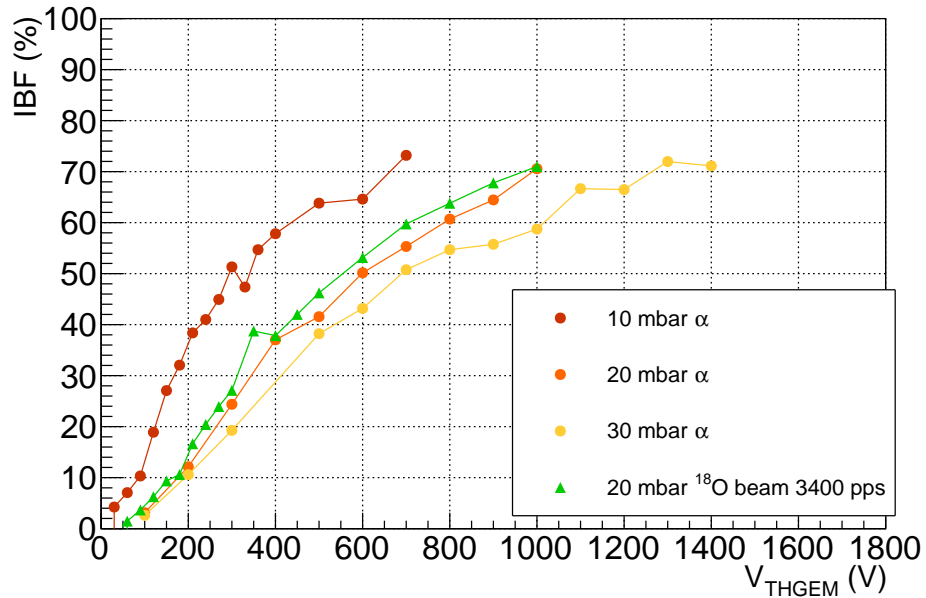


Figure 2.46: IBF for the ROW THGEM as a function of the  $\Delta V_{drift}$ . Run with  $\alpha$ -source and  $^{18}\text{O}$  beam are compared.

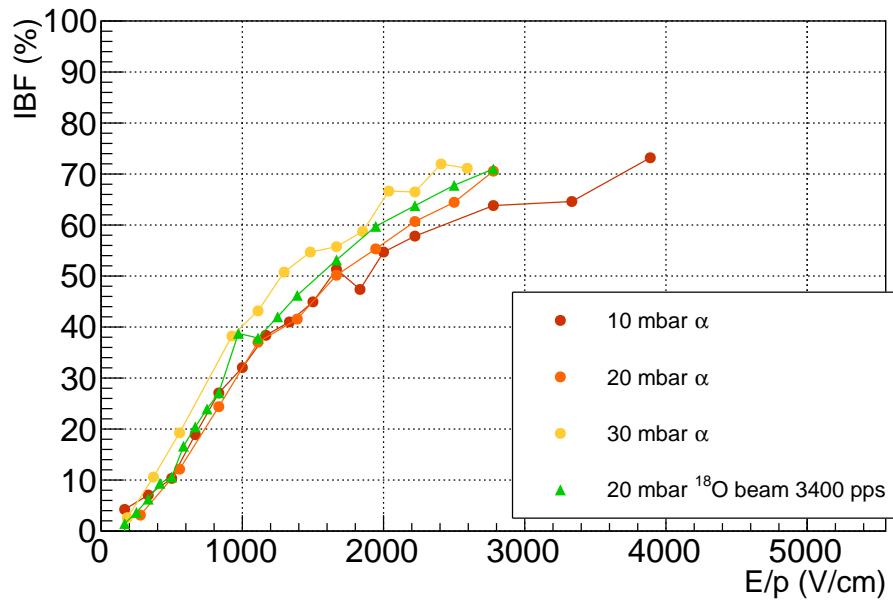


Figure 2.47: IBF for the ROW THGEM as a function of the reduced electric field. Run with  $\alpha$ -source and  $^{18}\text{O}$  beam are compared.

### Rate scan

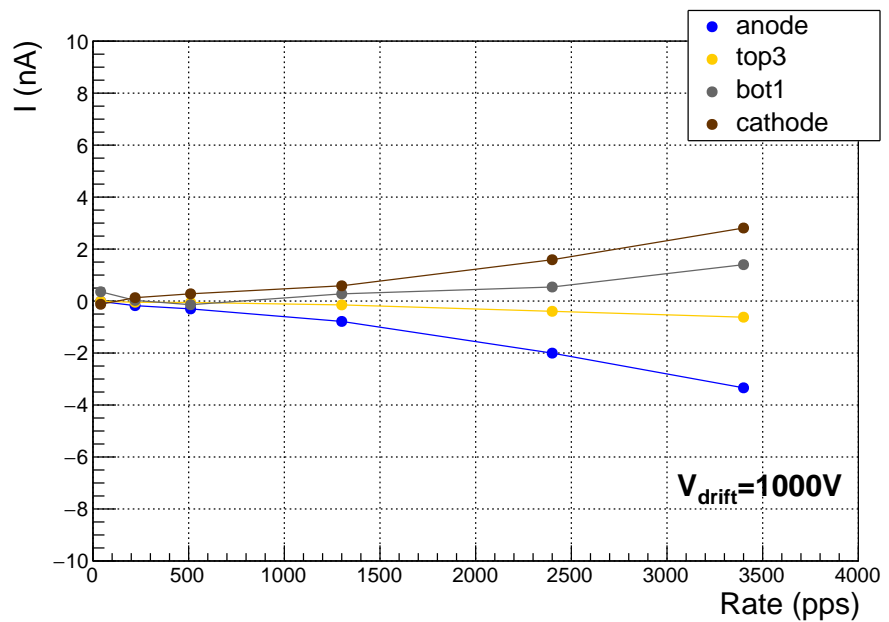


Figure 2.48: .

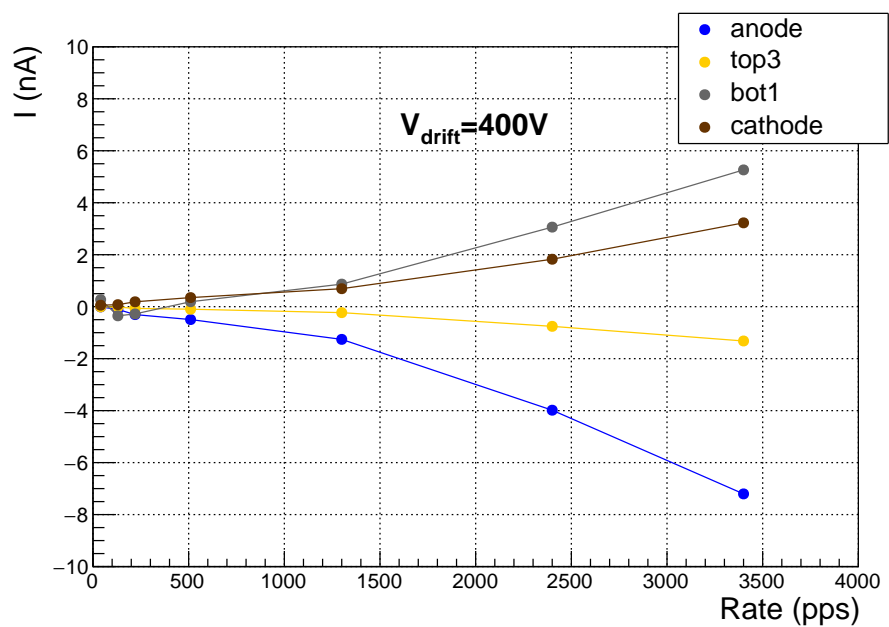


Figure 2.49: .

## .1 $^{241}\text{Am}$

$\alpha$ -decay 100% (spontaneous fission  $3.6 \times 10^{-12}$ ).  
 $^{241}\text{Am} \rightarrow ^{237}\text{Np} + ^4\text{He} + \gamma$   
 $\alpha$ -particles energy: 5.485 MeV (84.8%); 5.443 MeV (13.1%); 5.338 (2%)  
 $\gamma$ -ray 59.5 () 26.3 keV  
X-ray (L X-rays from Np) 20.7, 17.7, 16.9 and 13.9 keV

## .2 Geometria del rivelatore